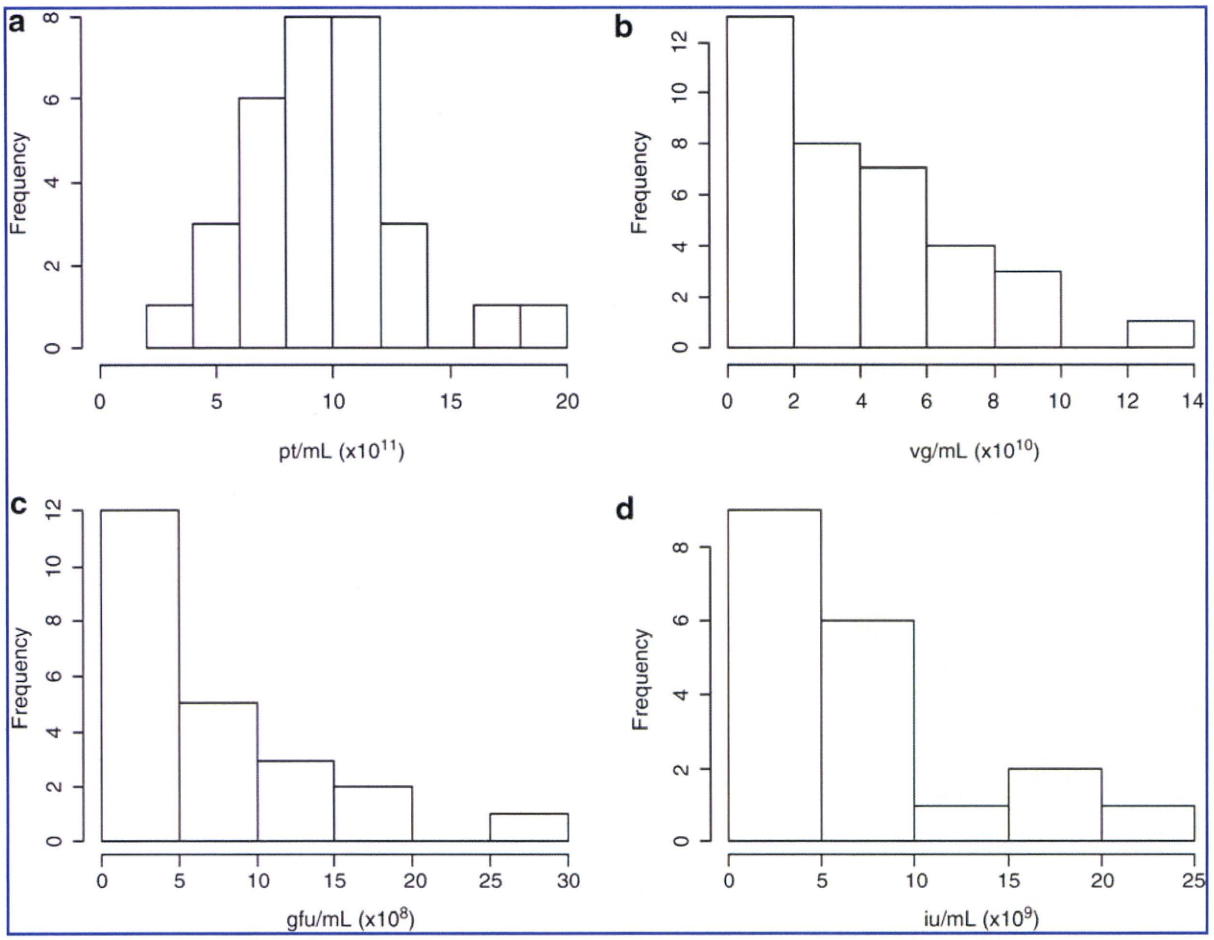

FIG. 1. Histograms displaying the distributions of (**a**) particle titer (pt/ml), (**b**) vector genome titer (VG/ml), (**c**) transducing titer (GFU/ml), and (**d**) infectious titer (IU/ml).

mally distributed. Because valid estimation of the mean and confidence interval relies on an underlying normal distribution, it was clear that some form of transformation was warranted. Common statistical transformation methods employed are square root, natural log, and log base 10. Means and intervals are calculated on the transformed data and the results are then back-transformed to the original measurement scale; the data for each assay were processed in this way, using all three transformations. Analysis of the mean and median (for normally distributed data these two values are the same) and skewness and kurtosis estimates confirmed that the transformations were performing as expected (data not shown). Figure 2 shows the results of the most successful transformations for each assay as quantile–quantile plots. In this analysis the quantiles (i.e., 5%, 10%, etc.) obtained from the transformed data are compared with the quantiles that would be expected for a normal distribution. A line that extends through the 25th and 75th quantile is shown on the plots and the nearer the points are to this line, the more normal the data distribution. With the exception of two extreme points, the capsid particle titer assay data appeared normally distributed without the need for transformation. For the vector genome titer and the transduction titer, square root transformation appeared to approximate normal distribution and seemed warranted. For the infectious titer, a log base 10 transformation appeared the most appropriate. The transformed data are summarized in Table 4. For each assay, 2 and 3 standard deviation limits were calculated corresponding to nominal 95 and 99.7% confidence bounds on individual values. Any test result lying outside of the 3 standard deviations was considered to be an outlier. Using this criterion only a single test result (from the particle titer assay) was determined to be an outlier and was removed from the analysis; the values reported in Table 4 exclude this data point.

An assumption we have made when calculating the mean values and confidence intervals is that each test result is independent of another; however, this assumption does not take into account that all institutions submitted duplicate (and in some cases triplicate) test results for the assays. To assess the degree of correlation between the two duplicate samples, Pearson coefficients were determined. These estimates ranged from 0.57 to 0.84 for the four assays (where a value of 1 indicates a perfect correlation). The results indicate that there is a significant correlation within institution and that the assumption that each result is independent is violated. To account for this correlation, the transformed data were modeled, using a linear random effect modeling approach (Littell *et al.*, 2006). This allows for a unique component associated with each institution to be included in the model, under the assumption that these institutional random effects have a mean of zero. When the correlation within an

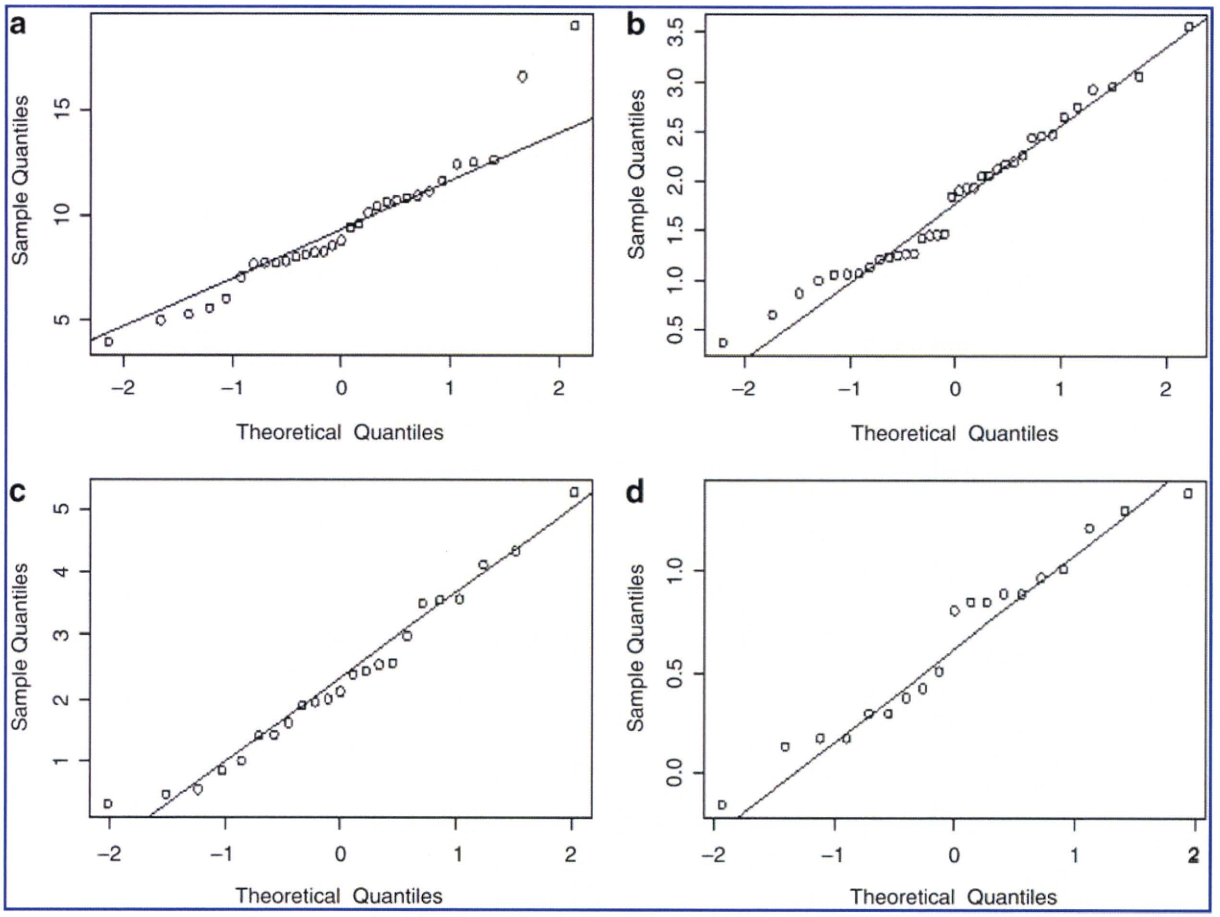

FIG. 2. Quantile–quantile plots displaying sample versus normal quantiles of (**a**) particles per milliliter, (**b**) square root of vector genomes per milliliter, (**c**) square root of transducing units per milliliter, and (**d**) $\log_{10}$ infectious units per milliliter. Lines pass through the 25th and 75th quantiles.

institution is accounted for, the precision of the mean estimate as illustrated by the width of the 95% confidence interval is decreased (Table 5). Taking the transformed, modeled data as the true estimate of the mean, we have arrived at the following determinations for the rAAV2 RSM: the mean particle titer is 9.18×10^{11} particles/ml with 95% confidence that the true value lies in the range of 7.89×10^{11} to 1.05×10^{12} particles/ml; the mean vector genome titer is 3.28×10^{10} vector genomes/ml with 95% confidence that the true value lies in the range of 2.70×10^{10} to 4.75×10^{10} vector genomes/ml; the mean transducing titer is 5.09×10^{8} transducing units/ml with 95% confidence that the true value lies in the range of 2.00×10^{8} to 9.60×10^{8} transducing units/ml; and the mean infectious titer is 4.37×10^{9} $TCID_{50}$ IU/ml with

TABLE 4. rAAV2 REFERENCE STANDARD MATERIAL TITER ESTIMATES AFTER TRANSFORMATION

Titer units (method)	*Transformation*[a]	*Mean*	*Lower 95% confidence limit for the mean*	*Upper 95% confidence limit for the mean*	*±2 SD*	*±3 SD*
Particles/ml (ELISA)	Untransformed	9.11×10^{11}	8.10×10^{11}	1.01×10^{12}	3.73×10^{11}–1.45×10^{12}	1.04×10^{11}–1.78×10^{12}
Vector genomes/ml (qPCR)	Square root	3.26×10^{10}	2.41×10^{10}	4.25×10^{10}	8.82×10^{8}–1.10×10^{11}	0–1.66×10^{11}
Transducing units/ml (green cells)	Square root	5.29×10^{8}	2.99×10^{8}	8.23×10^{8}	0–2.43×10^{9}	0–3.90×10^{9}
Infectious units/ml ($TCID_{50}$)	$\log_{10}$	4.49×10^{9}	2.75×10^{9}	7.29×10^{9}	5.94×10^{8}–3.39×10^{10}	2.16×10^{8}–9.31×10^{10}

[a]Used to better qualify the assumption of normal distribution for the purpose of determining distributional values.

TABLE 5. FINAL rAAV2 REFERENCE STANDARD MATERIAL TITER ESTIMATES AFTER TRANSFORMATION AND MODELING

Titer units (method)	*Transformation*[a]	*Mean*	*Lower 95% confidence limit for the mean*	*Upper 95% confidence limit for the mean*	*±2 SD*	*±3 SD*
Particles/ml (ELISA)	Untransformed	9.18×10^{11}	7.89×10^{11}	1.05×10^{12}	3.73×10^{11}–1.45×10^{12}	1.04×10^{11}–1.78×10^{12}
Vector genomes/ml (qPCR)	Square root	3.28×10^{10}	2.70×10^{10}	4.75×10^{10}	9.00×10^{8}–1.04×10^{11}	0–1.66×10^{11}
Transducing units/ml (green cells)	Square root	5.09×10^{8}	2.00×10^{8}	9.60×10^{8}	0–2.47×10^{9}	0–4.00×10^{9}
Infectious units/ml ($TCID_{50}$)	Log_{10}	4.37×10^{9}	2.06×10^{9}	9.26×10^{9}	5.15×10^{8}–3.71×10^{10}	1.77×10^{8}–1.08×10^{11}

[a]Used to better qualify the assumption of normal distribution for the purpose of determining distributional values.

95% confidence that the true value lies in the range of 2.06×10^{9} to 9.26×10^{9} $TCID_{50}$ IU/ml. The mean vector genome titer of 3.28×10^{10} VG/ml is almost 1 log lower than the titer of 2×10^{11} VG/ml assessed for the diluted purified bulk harvest before vialing. The discrepancy between the bulk material and final fill may be due to loss of vector after filtering of the bulk product, to the different assay methods used for the titering (dot–blot vs. qPCR), or a combination of both. The bulk vector was titered at the University of Florida, using the method of dot–blot hybridization to determine the appropriate formulation volume for the final fill. It is possible that the loss, if any, occurred during the final filtration and filling of the dilute reference standard material at the ATCC (diluted nearly 1000 times relative to preparations that are used preclinically or clinically). The product that was vialed and frozen constitutes the reference standard material that was characterized, and that is available to the community.

Some important properties of the rAAV2 RSM are indicated by the ratios of the titers (Table 6). The vector genome-to-infectious titer (VG:IU) ratio is often used as a measure of the relative infectivity of the vector, with lower ratios reflecting more infectious preparations. The rAAV2 RSM VG:IU ratio is 7.5, which indicates that the RSM has retained infectivity. The vector genome-to-transduction titer (VG:TU) ratio is 8.6-fold higher than the VG:IU ratio, and this result reflects the different sensitivities of the infectivity and transduction (measuring infectivity and gene expression) assays. Another ratio that is often used is the particle-to-vector genome titer ratio (P:VG). This ratio indicates the ratio of total particles, including both empty and full, to those particles containing the vector genome. The P:VG ratio obtained for the rAAV2 RSM is 28 and indicates a large excess of empty particles. This finding is consistent with the fact that the chromatographic purification process used in the production of the rAAV2 RSM was not designed to separate empty and full particles. One concern is that empty particles may have adversely affected the performance of the rAAV2 RSM in transduction and infectivity assays. However, during beta testing, two triple-transfected CsCl-purified lots (one each of AAV2.CMV.eGFP and AAV2.CMV.lacZ) were tested, using the RSS characterization methods: vector genome (qPCR), $TCID_{50}$, and where applicable eGFP transduction titering. Because these were CsCl-purified preparations the empty capsid content is lower than in preparations purified by chromatography. The VG:$TCID_{50}$ IU ratios and VG:TU ratios were similar or greater than those obtained for the reference standard (Tables 2 and 6). Similarly, the VG:$TCID_{50}$ IU ratios and VG:TU ratios of the reference standard (Table 6) are similar to those reported in the literature for other AAV2 vectors (Salvetti *et al.*, 1998; Zolotukhin *et al.*, 1999; Zen *et al.*, 2004).

TABLE 6. rAAV2 REFERENCE STANDARD MATERIAL TITER RATIOS

	Ratio
Particles: vector genomes[a]	27.99
Vector genomes: infectious units	7.51
Vector genomes: transducing units	64.44
Particles: infectious units	210.07

[a]A measure of the ratio of total particles to full particles.

The purity of the rAAV2 RSM was assessed and the capsid identity confirmed by SDS–PAGE analysis. The RSM was examined under both reducing and nonreducing conditions, using SYPRO ruby and silver stains (Fig. 3). Under reducing conditions all proteins including the denatured AAV2 capsids are expected to enter the gel and impurities would be detected as protein bands other than the capsid proteins VP1, VP2, and VP3. Under nonreducing conditions the capsid would remain intact and would not be expected to enter the resolving gel, whereas impurities would enter the gel; proteins that previously comigrated with the capsid proteins on reducing gels would thus be detected. Silver nitrate staining was included because it is capable of detecting DNA, lipid, and carbohydrate impurities as well as nanogram levels of protein (Weiss *et al.*, 2009). SYPRO ruby is a protein-specific fluorescent dye that has a sensitivity close to that of silver stain (Rabilloud *et al.*, 2001; Weiss *et al.*, 2009). In each case the rAAV2 RSM was analyzed alongside an internal laboratory standard AAV2 vector. The consensus data from the 11 testing laboratories that carried out the purity/identity test estimated that the rAAV2 RSM was greater than 94% pure and confirmed that VP1, VP2, and VP3 comigrated with the AAV2 capsid proteins of the internal vector standards (Fig. 3; and data not shown).

Discussion

As rAAV vectors more frequently head toward the clinic for gene therapy trials, there is an increasing need to share pharmacokinetic, toxicologic, and efficacy data. This need is

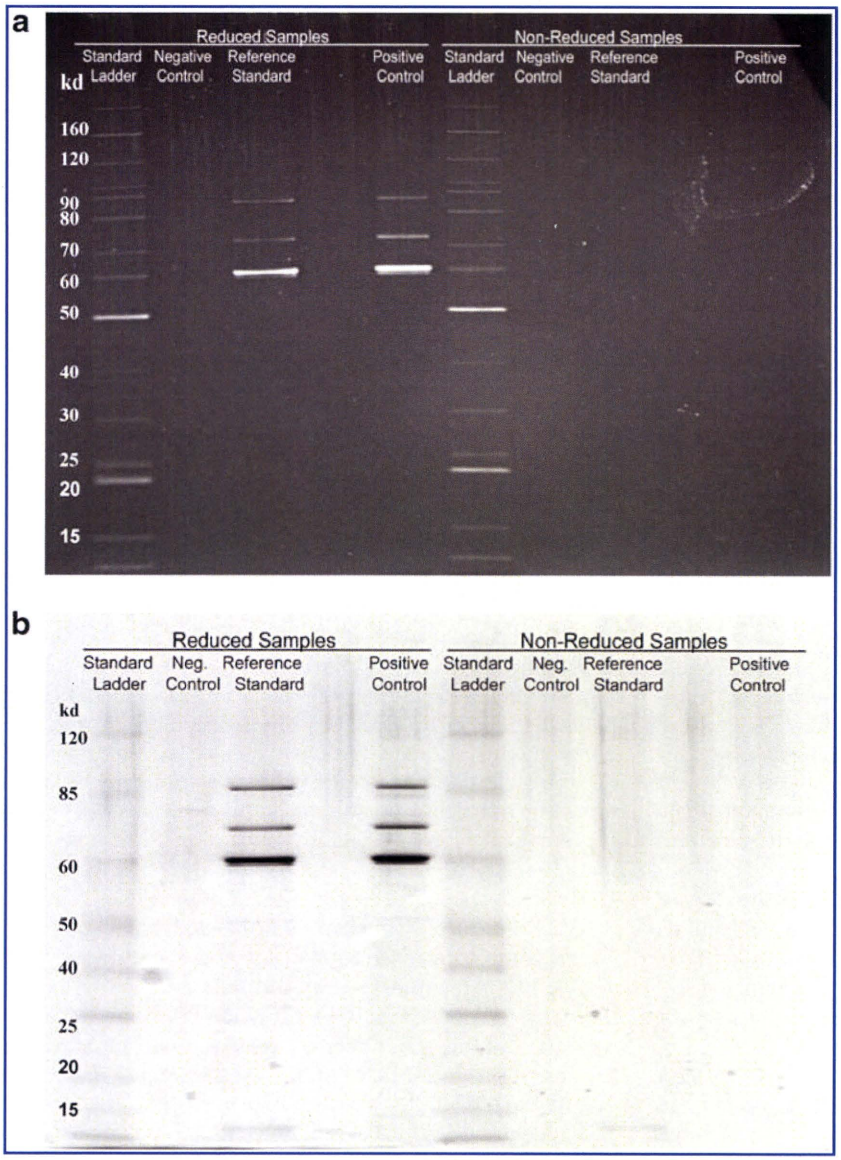

FIG. 3. The rAAV2 RSM was run on SDS–polyacrylamide gels under both reducing and native conditions and then stained with (**a**) SYPRO ruby or (**b**) silver stain. An in-house rAAV2 standard was run as a positive control and buffer as a negative control. The lanes for each gel are as follows: (1) benchmark ladder (unstained or prestained)—reduced; (2) negative control—reduced; (3) AAV reference material—reduced; (5) positive control—reduced; (6) benchmark ladder (unstained or prestained)—native; (7) negative control—native; (8) AAV reference material—native; (10) positive control—native.

currently confounded by the lack of standardization of critical vector parameters such as vector strength and potency. The standardization issues arise because different assays or different protocols for the same assay are often used by individual investigators to measure an identical vector property. The introduction of a widely accepted rAAV reference standard would allow laboratories to characterize AAV vectors in terms of common units, therefore facilitating comparison of doses determined by disparate assays and permitting safe and effective dosage at equivalent levels. Furthermore, efficacy and toxicology data reported in the literature could be used as a guide for initial dosing in animals and humans.

Here we have described the characterization of the first rAAV reference standard, an AAV serotype 2 vector. The goal of the AAV2RSWG was to provide a stable, high-quality, highly characterized RSM that would be both accepted and easily accessed by the AAV research community. As pointed out by FDA officials at the beginning of the effort, a reference standard material does not need to be pure or the "best," it just needs to be well characterized. Furthermore, there are many examples of viral reference standard materials from the World Health Organization (WHO, Geneva, Switzerland) and the National Institute for Biological Standards and Control (NIBSC, Potters Bar, UK) that are not pure (e.g., poliovirus and hepatitis B virus references). Although the rAAV2 RSM was made in a research vector core and not at a current Good Manufacturing Procedure (cGMP) facility, it was extensively tested for adventitious agents and contaminants. The final rAAV2 RSM product was negative for adventitious agents in all tests to which it was subjected, although the harvest material was exposed to mycoplasma that was cleared and/or inactivated in the purification process, because the purified bulk tested negative for viable mycoplasma and mycoplasma DNA (Potter *et al.*, 2008). Because the rAAV2 RSM is a reference standard to be used in research and quality control (QC) laboratories and is not intended for use in humans, the AAV2RSWG recommended that filling, banking, and characterization proceed. A summary of the mycoplasma testing will be included on the

product information sheet supplied with each shipment of the rAAV2 RSM, stating that the reference standard has been exposed to mycoplasma, but is mycoplasma-free. Thus, institutions and companies requesting the rAAV2 RSM will be fully informed and can decide if they want to bring it into their QC laboratories. The reference material is intended to be restricted to QC laboratories, isolated from production suites. In addition, it is envisioned that internal reference standards will be calibrated against the AAV2 RSM one time and then used on a routine basis for product-specific testing.

The short-term stability testing performed on the surrogate AAV2-GFP vector as well as on the final vialed rAAV2 RSM material suggested that some loss of vector potency was occurring on storage. Initially this loss was assumed to be due to absorption to the surfaces of the vial as was seen in the previous study using vials that were not siliconized (Potter *et al.*, 2008); however, when vector genomes were assayed no corresponding loss was seen when using siliconized vials (Table 2). One explanation for the loss of potency observed may be the omission of a stabilizing excipient in the final formulation (Croyle *et al.*, 2001; Wright *et al.*, 2003). The beta test stability results influenced the way the rAAV2 RSM was handled during the testing phase; aliquots were thawed only once and transduction and infectivity assays were performed within 1 hr of this thaw. Regarding future use of the reference material for potency assays, it would seem essential that a similar protocol be followed when normalizing internal reference standards against the rAAV2 RSM. For physical titer assays such as particle and vector genome assays, storage and refreezing are permissible. Plans for assessing the long-term stability of the rAAV2 RSM by yearly testing for capsid protein integrity, infectious titer, transducing titer, and vector genome titer are in place. Data will be reported by the AAV2RSWG through the Reference Standards section of the International Society for BioProcess Technology website (www.ISBioTech.org).

The characterization phase of the rAAV2 RSM project successfully fulfilled the goals of the AAV2RSWG by obtaining mean titers and 95% confidence intervals from a large number of representative assays performed by numerous test centers. The tightest confidence intervals were obtained for the nonbiological assays (particle titer and vector genome titer) whereas the biological assays (infectious titer and transduction titer) gave wider intervals (Table 5). This pattern might be expected because the biological assays are inherently more variable. The tight confidence interval observed for the vector genome titer is relevant because this titer has been used exclusively in dosing regimens and a high degree of precision is important for the use of the rAAV2 RSM in dose standardization.

One obvious trend in the quantitative assay data was the degree of variation between institutions for each assay (Fig. 1 and Table 3) despite the relatively tight correlation of assay results within an institution (Table 3). This poor degree of interlaboratory precision and accuracy was apparent even though attempts were made to standardize the assays by providing detailed protocols and common reagents. The variation may be explained by the use of different reagents (i.e., other than those provided, such as tissue culture media, PCR primers, and PCR mixes), equipment, and/or operator technique. This is the first time that such variation between laboratories has been thoroughly documented and the findings emphasize the need in the field for universal reference standards. This need is especially apparent when it is considered that fundamentally dissimilar tests are often used to measure the same parameter (e.g., qPCR and dot–blot for vector genome titer) and that even when different laboratories use the same assay, different protocols are usually followed. For some assays the variation is not large, with the most important measure, vector genome titer (qPCR), which is almost exclusively used for dosing in preclinical and clinical studies, having low variation (confidence interval of less than 0.5 log). Despite the spread of infectious titers, the mean value represents the best titer based on multiple replicates conducted at the different sites on different test dates.

Because the rAAV2 RSM supply is limited, it is not intended that it be used routinely, but rather for the calibration of laboratory-specific internal reference standards, which can then be run concurrently with test samples in subsequent assays that have been validated. The initial calibration would involve titering the RSM alongside the internal standard in the same assay; the difference between the titer determined in this assay and the accepted titer of the RSM would act as a conversion factor for calculating the titer of the internal standard in reference standard units (RSU). Once the internal standard titer is known in reference standard units per milliliter, the titer of test samples can be calculated similarly in the same units, during subsequent assays. It is envisaged that the RSM will be used in this way for standardizing the genome titer, particle titer, and infectious titer of AAV2 vectors. A prerequisite for qPCR or hybridization-based vector genome/infectivity titering methods would be that the internal AAV standard share enough genome sequence with the rAAV2 RSM for oligonucleotide or labeled probe annealing. Several common transcriptional elements are included in the rAAV2 RSM genome for this purpose and many existing internal reference standards will therefore be candidates for calibration. If this is not the case, new internal standards will need to be produced that harbor DNA elements in common with the AAV2 RSM. For transducing titers, the encoded transgene provides the basis of detection and, therefore, with the exception of GFP-expressing vectors for preclinical studies, these titers will generally not be amenable to standardization using the rAAV2 RSM.

Although the primary intent of the rAAV2 RSM was to provide a reference point for AAV2 serotype vectors it is possible that for nonbiological assays such as vector genome titration, the rAAV2 RSM could be used for the calibration of other AAV serotypes. Because the vector capsid is not directly involved in these types of assays, it might be argued that there is no capsid specificity and that the capsid serotype would not have an impact. As an example, in the vector genome titer assay it might be assumed that different capsids are equally susceptible to PCR heat treatment for liberation of the vector genome. However, conditions would need to be optimized because equal susceptibility of AAV serotypes to heat has not been definitively demonstrated. In addition, proteolysis is often used to liberate the vector genome and it is known that different capsid serotypes have different susceptibilities to protease treatments (Van Vliet *et al.*, 2006). Similarly, serotype-independent methods of determining particle titer (e.g., high-performance liquid chromatography, spectrophotometry) could be calibrated, using the rAAV2 RSM, but the same assumption of capsid independence

would apply, and for spectrophotometric measurements the proper extinction coefficient would need to be incorporated (Sommer *et al.*, 2003). If data are available to demonstrate that an assay is indeed capsid independent, then the use of the rAAV2 RSM for other serotypes may well be acceptable, but thorough review with the appropriate regulatory agency is recommended. For biological assays such as infectious titer, the paramount roles of the capsid, the requisite target cell line, and the helper virus preclude the use of the rAAV2 RSM to calibrate other serotypes. For these assays, investigators must await the development of further reference standard materials such as the AAV8 material currently under production (Moullier and Snyder, 2008).

The rAAV2 RSM carries a single-stranded DNA vector genome. Self-complementary AAV vector genomes, generated with a mutation within the terminal repeat (McCarty *et al.*, 2003), have become popular for gene transfer because they bypass the rate-limiting genome conversion of single-stranded to double-stranded DNA during transduction of target cells. The rAAV2 RSM can be used to normalize "in-house" reference standards for both the classic single-stranded vectors and self-complementary vectors. Because self-complementary vectors carry double the genome complement of single-stranded vectors, a simple conversion is necessary when calculating vector genome titers for these two vector types.

In the United States, the FDA Center for Biologics Evaluation and Research (CBER), Office of Cellular, Tissue, and Gene Therapies (OCTGT), Division of Cellular and Gene Therapies (DCGT) recommends reference materials as benchmarking tools for qualifying and validating "in-house" reference standards and assays by comparison with the collective data. It should be noted that it is not the intent of the FDA to standardize assay methods across the field or to require that the values assigned to the rAAV2RSM be duplicated during validation studies. Furthermore, there is no requirement in the United States to follow rAAV2 RSM procedures when assaying particle concentration, genome copy number, or infectious titer. Sponsors of adeno-associated virus-related investigational new drugs (INDs) should consult with the FDA/CBER or appropriate national agency for further guidance. The rAAV2 RSM fulfills many of the requirements of a reference standard material in that it (1) is sufficiently homogeneous and stable with respect to specified properties, (2) is established to be fit for its intended use in measurement, (3) is accompanied by documentation, (4) provides relevant property values that are based on multiple measurements conducted at different locations, and (5) is accompanied with associated measurement uncertainty.

From the outset, the vision of the AAV2RSWG for the rAAV2 RSM was that it would represent the first step toward standardization of AAV-based gene therapy dosing and provide a blueprint for the development of reference standards for other AAV serotypes. This vision is becoming reality through the successful production and characterization reported here, and with the effort to develop the AAV8 reference standard material underway. The requirement that the reference materials be universally accepted by the AAV community has dictated the need for a voluntary communal effort in the production and characterization phases. Despite the numerous drawbacks, difficulties, and delays inherent in this type of approach, the AAV gene therapy community has responded selflessly and with enthusiasm. It is hoped that the ultimate success of this collaboration will inspire future reference standard efforts and contribute to the development and commercialization of AAV-based gene therapeutics.

Acknowledgments

Current and former members of the Executive Committee: Denise Gavin–FDA (nonvoting member); Daniel Rosenblum–NIH NCRR (nonvoting member); Keith Carson–International Society for BioProcess Technology; Parris Burd–Bayer Corporation; Olivier Danos–Généthon; Maritza McIntyre–FDA (nonvoting member); Richard Knazek–NIH NCRR (nonvoting member). Manufacturing committee: Guang Ping Gao–University of Pennsylvania; Philip Cross–Harvard Medical School; Anna Salvetti–CHU Hôtel Dieu, Nantes, France; Sue Washer–Applied Genetic Technologies; Guang Qu–Avigen. Quality committee: Marie Printz–Ceregene; Paul Husak–Cell Genesys; Scott McPhee–Thomas Jefferson University; Jurg Sommer–Avigen; Jim Marich–Cell Genesys. We acknowledge the technical help of the following during the testing phase: Mark Potter–PGTC Vector Core; Gitte Kitlen–PGTC Quality Control; Lynn Combee–PGTC Toxicology Core; Cheryl Roberts–PGTC Toxicology Core; Tanja Finnäs–AMT; Martha Hoekstra–AMT. We are grateful to James Wilson–University of Pennsylvania for supporting the beta testing through NIH grant P30-DK-047757 and an SRA from GlaxoSmithKline. We are also indebted to Peggy Fahnestock and Liz Kerrigan at the ATCC for coordinating the distribution of materials to testing laboratories. This work was supported by NIH grant U42RR11148. We acknowledge the generosity of the ATCC, Nunc, Aldevron, Corning, Fisher Thermo Scientific, the Indiana University Vector Production Facility, HyClone, Mediatech, Progen, and the Williamsburg Bioprocessing Foundation. Richard Surosky is employed by a company that may have interest in these vectors for therapeutic purposes. Richard Snyder owns equity in a gene therapy company that is commercializing AAV for gene therapy applications.

References

Brantly, M.L., Chulay, J.D., Wang, L., Mueller, C., Humphries, M., Spencer, L.T., Rouhani, F., Conlon, T.J., Calcedo, R., Betts, M.R., Spencer, C., Byrne, B.J., Wilson, J.M., and Flotte, T.R. (2009). Sustained transgene expression despite T lymphocyte responses in a clinical trial of rAAV1-AAT gene therapy. Proc. Natl. Acad. Sci. U.S.A. 106, 16363–16368.

Burger, C., Gorbatyuk, O.S., Velardo, M.J., Peden, C.S., Williams, P., Zolotukhin, S., Reier, P.J., Mandel, R.J., and Muzyczka, N. (2004). Recombinant AAV viral vectors pseudotyped with viral capsids from serotypes 1, 2, and 5 display differential efficiency and cell tropism after delivery to different regions of the central nervous system. Mol. Ther. 10, 302–317.

CBER/FDA (Center for Biologics Evaluation and Research, U.S. Food and Drug Administration). (1993). Points to consider in the characterization of cell lines used to produce biologicals. Available at http://www.fda.gov/downloads/BiologicsBloodVaccines/GuidanceComplianceRegulatoryInformation/OtherRecommendationsforManufacturers/UCM062745.pdf (accessed July 2010).

Chadeuf, G., Favre, D., Tessier, J., Provost, N., Nony, P., Kleinschmidt, J., Moullier, P., and Salvetti, A. (2000). Efficient

recombinant adeno-associated virus production by a stable rep-cap HeLa cell line correlates with adenovirus-induced amplification of the integrated rep-cap genome. J. Gene Med. 2, 260–268.

Croyle, M.A., Cheng, X., and Wilson, J.M. (2001). Development of formulations that enhance physical stability of viral vectors for gene therapy. Gene Ther. 8, 1281–1290.

Grimm, D., Kern, A., Rittner, K., and Kleinschmidt, J.A. (1998). Novel tools for production and purification of recombinant adenoassociated virus vectors. Hum. Gene Ther. 9, 2745–2760.

Hutchins, B. (2002). Development of a reference material for characterizing adenovirus vectors. BioProcess. J. 1, 25–28.

Kärber, G. (1931). 50% end-point calculation. Arch. Exp. Pathol. Pharmak. 162, 480–483.

Littell, R.C., Milliken, G.A., Stroup, W.W., and Wolfinger, R.E. (2006). *SAS for Mixed Models*, 2nd ed. (SAS Institute, Cary, NC).

Maguire, A.M., Simonelli, F., Pierce, E.A., Pugh, E.N., Jr., Mingozzi, F., Bennicelli, J., Banfi, S., Marshall, K.A., Testa, F., Surace, E.M., Rossi, S., Lyubarsky, A., Arruda, V.R., Konkle, B., Stone, E., Sun, J., Jacobs, J., Dell'Osso, L., Hertle, R., Ma, J.X., Redmond, T.M., Zhu, X., Hauck, B., Zelenaia, O., Shindler, K.S., Maguire, M.G., Wright, J.F., Volpe, N.J., McDonnell, J.W., Auricchio, A., High, K.A., and Bennett, J. (2008). Safety and efficacy of gene transfer for Leber's congenital amaurosis. N. Engl. J. Med. 358, 2240–2248.

McCarty, D.M., Fu, H., Monahan, P.E., Toulson, C.E., Naik, P., and Samulski, R.J. (2003). Adeno-associated virus terminal repeat (TR) mutant generates self-complementary vectors to overcome the rate-limiting step to transduction *in vivo*. Gene Ther. 10, 2112–2118.

Moss, R.B., Rodman, D., Spencer, L.T., Aitken, M.L., Zeitlin, P.L., Waltz, D., Milla, C., Brody, A.S., Clancy, J.P., Ramsey, B., Hamblett, N., and Heald, A.E. (2004). Repeated adeno-associated virus serotype 2 aerosol-mediated cystic fibrosis transmembrane regulator gene transfer to the lungs of patients with cystic fibrosis: A multicenter, double-blind, placebo-controlled trial. Chest 125, 509–521.

Moullier, P., and Snyder, R.O. (2008). International efforts for recombinant adeno-associated viral vector reference standards. Mol. Ther. 16, 1185–1188.

Mueller, C., and Flotte, T.R. (2008). Clinical gene therapy using recombinant adeno-associated virus vectors. Gene Ther. 15, 858–863.

Nienhuis, A. (2009). Dose-escalation study of a self complementary adeno-associated viral vector for gene transfer in hemophilia B. Clinical trial NCT00979238. Available at http://clinicaltrials.gov/ct2/show/NCT00979238 (accessed July 2010).

Potter, M., Phillipsberg, G., Phillipsberg, T., Pettersen, M., Sanders, D., Korytov, I., Fife, J., Zolotukhin, S., Byrne, B.J., and Muzyczka, N. (2008). Manufacture and stability study of the recombinant adeno-associated virus serotype 2 vector reference standard. Bioprocess. J. 7, 8–14.

Rabilloud, T., Strub, J.M., Luche, S., van Dorsselaer, A., and Lunardi, J. (2001). A comparison between SYPRO Ruby and ruthenium II tris(bathophenanthroline disulfonate) as fluorescent stains for protein detection in gels. Proteomics 1, 699–704.

Salvetti, A., Oreve, S., Chadeuf, G., Favre, D., Cherel, Y., Champion-Arnaud, P., David-Ameline, J., and Moullier, P. (1998). Factors influencing recombinant adeno-associated virus production. Hum. Gene Ther. 9, 695–706.

Snyder, R.O., and Flotte, T.R. (2002). Production of clinical-grade recombinant adeno-associated virus vectors. Curr. Opin. Biotechnol. 13, 418–423.

Sommer, J.M., Smith, P.H., Parthasarathy, S., Isaacs, J., Vijay, S., Kieran, J., Powell, S.K., McClelland, A., and Wright, J.F. (2003). Quantification of adeno-associated virus particles and empty capsids by optical density measurement. Mol. Ther. 7, 122–128.

Van Vliet, K., Blouin, V., Agbandje-McKenna, M., and Snyder, R.O. (2006). Proteolytic mapping of the adeno-associated virus capsid. Mol. Ther. 14, 809–821.

Warrington, K.H., Jr., and Herzog, R.W. (2006). Treatment of human disease by adeno-associated viral gene transfer. Hum. Genet. 119, 571–603.

Weiss, W., Weiland, F., and Gorg, A. (2009). Protein detection and quantitation technologies for gel-based proteome analysis. Methods Mol. Biol. 564, 59–82.

Wright, J.F., Qu, G., Tang, C., and Sommer, J.M. (2003). Recombinant adeno-associated virus: Formulation challenges and strategies for a gene therapy vector. Curr. Opin. Drug Discov. Dev. 6, 174–178.

Zen, Z., Espinoza, Y., Bleu, T., Sommer, J.M., and Wright, J.F. (2004). Infectious titer assay for adeno-associated virus vectors with sensitivity sufficient to detect single infectious events. Hum. Gene Ther. 15, 709–715.

Zolotukhin, S., Byrne, B.J., Mason, E., Zolotukhin, I., Potter, M., Chesnut, K., Summerford, C., Samulski, R.J., and Muzyczka, N. (1999). Recombinant adeno-associated virus purification using novel methods improves infectious titer and yield. Gene Ther. 6, 973–985.

Address correspondence to:
Dr. Richard O. Snyder
Department of Molecular Genetics and Microbiology
1600 SW Archer Road
Gainesville, FL 32610-0266

E-mail: rsnyder@cerhb.ufl.edu

Received for publication December 21, 2009;
accepted after revision May 18, 2010.

Published online: August 25, 2010.

This article has been cited by:

1. W Ni, C Le Guiner, G Gernoux, M Penaud-Budloo, P Moullier, R O Snyder. 2011. Longevity of rAAV vector and plasmid DNA in blood after intramuscular injection in nonhuman primates: implications for gene doping. *Gene Therapy* . [CrossRef]
2. V. Jimenez, E. Ayuso, C. Mallol, J. Agudo, A. Casellas, M. Obach, S. Muñoz, A. Salavert, F. Bosch. 2011. In vivo genetic engineering of murine pancreatic beta cells mediated by single-stranded adeno-associated viral vectors of serotypes 6, 8 and 9. *Diabetologia* . [CrossRef]
3. Cormac Sheridan. 2011. Gene therapy finds its niche. *Nature Biotechnology* **29**:2, 121-128. [CrossRef]
4. Hiroya Yagi, Tsuyoshi Ogura, Hiroaki Mizukami, Masashi Urabe, Hiromi Hamada, Hiroyuki Yoshikawa, Keiya Ozawa, Akihiro Kume. 2011. Complete restoration of phenylalanine oxidation in phenylketonuria mouse by a self-complementary adeno-associated virus vector. *The Journal of Gene Medicine* n/a-n/a. [CrossRef]

nature biotechnology

Generation of induced pluripotent stem cells without Myc from mouse and human fibroblasts

Masato Nakagawa[1,5], Michiyo Koyanagi[1,5], Koji Tanabe[1], Kazutoshi Takahashi[1], Tomoko Ichisaka[1,2], Takashi Aoi[1], Keisuke Okita[1], Yuji Mochiduki[1], Nanako Takizawa[1] & Shinya Yamanaka[1,2,3,4]

Direct reprogramming of somatic cells provides an opportunity to generate patient- or disease-specific pluripotent stem cells. Such induced pluripotent stem (iPS) cells were generated from mouse fibroblasts by retroviral transduction of four transcription factors: Oct3/4, Sox2, Klf4 and c-Myc[1]. Mouse iPS cells are indistinguishable from embryonic stem (ES) cells in many respects and produce germline-competent chimeras[2–4]. Reactivation of the c-Myc retrovirus, however, increases tumorigenicity in the chimeras and progeny mice, hindering clinical applications[3]. Here we describe a modified protocol for the generation of iPS cells that does not require the Myc retrovirus. With this protocol, we obtained significantly fewer non-iPS background cells, and the iPS cells generated were consistently of high quality. Mice derived from Myc$^-$ iPS cells did not develop tumors during the study period. The protocol also enabled efficient isolation of iPS cells without drug selection. Furthermore, we generated human iPS cells from adult dermal fibroblasts without MYC.

This study was initiated to examine whether the family proteins of the four transcription factors could generate iPS cells. Mouse embryonic fibroblasts (MEFs) containing a green fluorescent protein (GFP)-IRES-Puro^r transgene driven by the Nanog gene regulatory elements were used[3]. Nanog is specifically expressed in mouse ES cells and preimplantation embryos[5,6] and can serve as a selection marker during iPS cell induction. Introduction of the aforementioned four factors reprograms MEFs to GFP-expressing colonies of iPS cells. Nanog-selected iPS cells are indistinguishable from ES cells in morphology, proliferation and gene expression, and give rise to germline-competent chimeras[2–4].

Oct3/4 belongs to the octamer-binding (Oct) family of transcription factors, which contain the POU domain[7]. The closest homologs of Oct3/4 are Oct1 and Oct6. We introduced Oct3/4, Oct1 or Oct6, together with the remaining three factors, into the Nanog-reporter MEFs by retroviral delivery. With Oct3/4, many GFP$^+$ colonies were observed (**Fig. 1a**). In contrast, no GFP$^+$ colonies were obtained with Oct1 or Oct6, thus indicating the inability of these two homologs to induce iPS cells. Sox2 is one of the SRY-related HMG-box (Sox) transcription factors, characterized by the presence of the high-mobility group (HMG) domain[8]. We tested Sox1, Sox3, Sox7, Sox15, Sox17 and Sox18. GFP$^+$ colonies were obtained with Sox1, and fewer GFP$^+$ colonies were obtained with Sox3, Sox15 and Sox18 (**Fig. 1a**). Sox18, however, failed to expand the cells. Klf4 belongs to the family of Krüppel-like factors (Klfs), zinc-finger proteins that contain amino acid sequences similar to those of the *Drosophila* embryonic pattern regulator Krüppel[9]. Klf1, Klf2 and Klf5 were tested, and GFP-expressing colonies were obtained with Klf2 (**Fig. 1a**). Klf1 and Klf5 also generated iPS cells, but with a lower efficiency. c-Myc has two related proteins: N-Myc and L-Myc[10]. GFP$^+$ colonies emerged with both N-Myc and L-Myc (**Fig. 1a**). Therefore, some, but not all, family proteins of the four factors can reprogram MEFs to iPS cells.

We also tested the family proteins for their ability to reprogram MEFs in which βgeo (a fusion between β-galactosidase and the neomycin-resistance gene) was knocked into the *Fbxo15* locus[11]. Similar results to those with the Nanog-based selection were obtained: Sox2 could be replaced by Sox1 and Sox3, Klf4 by Klf2, and c-Myc by N-Myc and L-Myc. The cells generated by the family proteins were expandable and showed a morphology indistinguishable from that of ES cells (not shown). They gave rise to teratomas in nude mice (see **Supplementary Fig. 1** online). Therefore, some family proteins are capable of inducing iPS cells from both Nanog-reporter MEFs and Fbxo15-reporter MEFs.

Unexpectedly, a few ES cell–like and GFP$^+$ colonies from Nanog-reporter MEFs were obtained without the Myc retrovirus (**Fig. 1a**). This was in contrast to a previous study in which no GFP$^+$ colonies could be obtained without Myc[3]. One difference between the two studies is the timing of the drug selection. In the earlier study, puromycin selection was initiated 7 d after the transduction, whereas in the present experiment the selection was started 14 d after. This suggested that iPS cell generation without Myc is slower than with Myc.

To test this possibility, we transduced Nanog-reporter MEFs either with the four factors or with three factors devoid of Myc, and started puromycin selection 7, 14 or 21 d after transduction (**Fig. 1b**). With the four

[1]Department of Stem Cell Biology, Institute for Frontier Medical Sciences, Kyoto University, Kyoto 606-8507, Japan. [2]CREST, Japan Science and Technology Agency, Kawaguchi 332-0012, Japan. [3]Gladstone Institute of Cardiovascular Disease, San Francisco, CA 94158, USA. [4]Institute for Integrated Cell-Material Sciences, Kyoto University, Kyoto 606-8507, Japan. [5]These authors contributed equally to this work. Correspondence should be addressed to S.Y. (yamanaka@frontier.kyoto-u.ac.jp).

Received 6 November; accepted 23 November; published online 30 November 2007; doi:10.1038/nbt1374

factors, GFP$^+$ colonies were observed in all of the conditions. The colony numbers substantially increased when puromycin selection was delayed. Without Myc, no GFP$^+$ colonies were observed when selection was initiated 7 d after transduction. In contrast, GFP$^+$ colonies did emerge even without Myc when selection was started 14 or 21 d after transduction. In each condition there were fewer colonies with the three factors than with the four factors. Nanog-selected iPS cells generated without the Myc retrovirus expressed ES-cell marker genes at similar levels to those in ES cells (**Supplementary Fig. 2** online), and gave rise to adult chimeras when transplanted into blastocysts (**Supplementary Table 1** online). Another difference is that fewer GFP$^-$ colonies and fewer background cells were observed with the three factors devoid of Myc than with the four factors (**Fig. 1c**). Therefore, the omission of Myc resulted in a less efficient but more specific induction of MEFs to iPS cells.

In the present study, it was also possible to generate a few iPS cells without Myc from MEFs in which βgeo was knocked into the *Fbxo15* locus[11] (**Fig. 2a**). This is again in contrast to the original report, in which no iPS cells were obtained without Myc[1]. In the two experiments, G418 selection was initiated with the same timing: 3 d after the transduction. However, the colonies appeared 14–21 d after transduction of the four factors, whereas ~30 d were required without the Myc retrovirus. Another difference was that in the present study the retroviral transfection efficiency was increased by preparing each of the four or three factors separately in an independent Plat-E[12] plate. This yielded a significant increase in the number of iPS cell colonies compared with the original work, in which all four factors were prepared in a single Plat-E plate. This result is consistent with the notion that generation of iPS cells without Myc is a slower and less efficient process than with Myc.

Fbxo15-selected iPS cells generated with the four factors express lower levels of ES-cell marker genes than do ES cells[1]. They cannot produce adult chimeras when microinjected into blastocysts. In contrast, iPS cells generated without Myc expressed ES-cell marker genes at similar levels to those in ES cells even with the Fbxo15 selection (**Fig. 2b**). Furthermore, adult chimeras with a high contribution from these iPS cells were obtained (**Fig. 2c** and **Supplementary Table 1**).

We examined tumorigenicity in these mice derived from the Myc$^-$ iPS cells, which were selected for either Nanog or Fbxo15 (**Supplementary Table 1**). We found that six of 37 chimeras derived from iPS cells with the four factors died of tumors within 100 d after birth. By contrast, all 26 chimeras generated without Myc survived this period (**Fig. 2d**). Thus, the omission of the Myc retrovirus significantly reduced the risk of tumorigenicity in chimeras ($P < 0.05$ by χ^2 test). Future study is required to determine whether these mice develop tumors later in life.

Next, we examined whether the omission of Myc would result in efficient isolation of iPS cells without drug selection. The four or three factors were introduced into adult tail tip fibroblasts (TTFs) containing the Nanog reporter, but puromycin selection was not applied. To visualize transduced cells, we used DsRed retrovirus together with the four or three factors. Thirty days after the retroviral transduction, the dishes with cells transduced with the four factors were covered with numerous GFP$^-$ colonies and background cells (**Fig. 3a** and **Supplementary Table 2** online). Using fluorescence microscopy, we found small portions of these colonies (4, 132 and 424 colonies in three independent experiments) to be GFP$^+$. Of note, the GFP$^+$ colonies were negative for DsRed, which was consistent with the retroviral silencing observed in Nanog-selected iPS cells[3]. In contrast, with the three factors devoid of Myc, a small number (7, 21 and 43 in three independent experiments) of discrete colonies was observed with few background cells. Approximately half of them expressed GFP

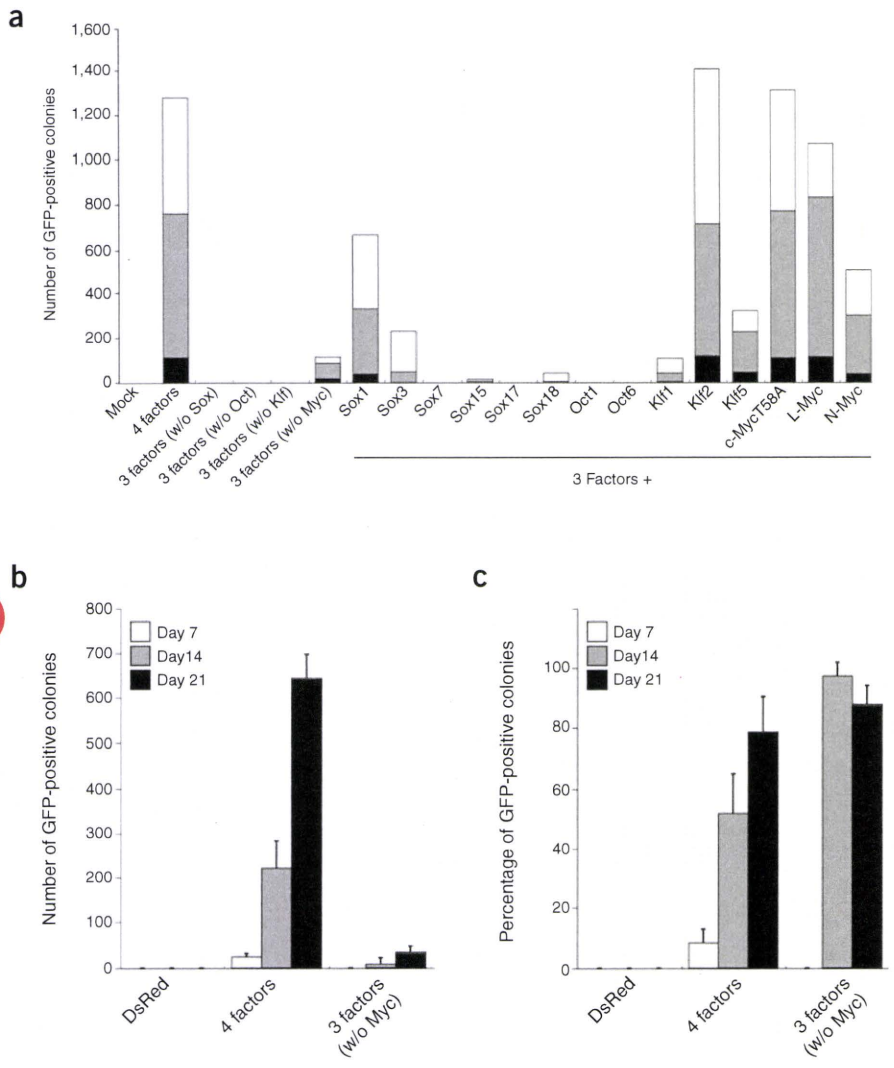

Figure 1 Effect of family factors and omission of Myc on the generation of iPS cells from Nanog-reporter MEFs. (**a**) Generation of iPS cells with family genes from MEFs by Nanog selection. The number of GFP$^+$ colonies is shown. The results of three independent experiments are shown with different colors (white, gray and black). "4 factors" indicates the combination of Oct3/4, Sox2, Klf4 and c-Myc. (**b**) The effect of puromycin selection timing on iPS cell generation. Shown are GFP$^+$ colonies observed 28 d after transduction of the four factors or the three factors devoid of Myc. (**c**) The effect of puromycin selection timing on the percentage of GFP$^+$ colonies per all colonies.

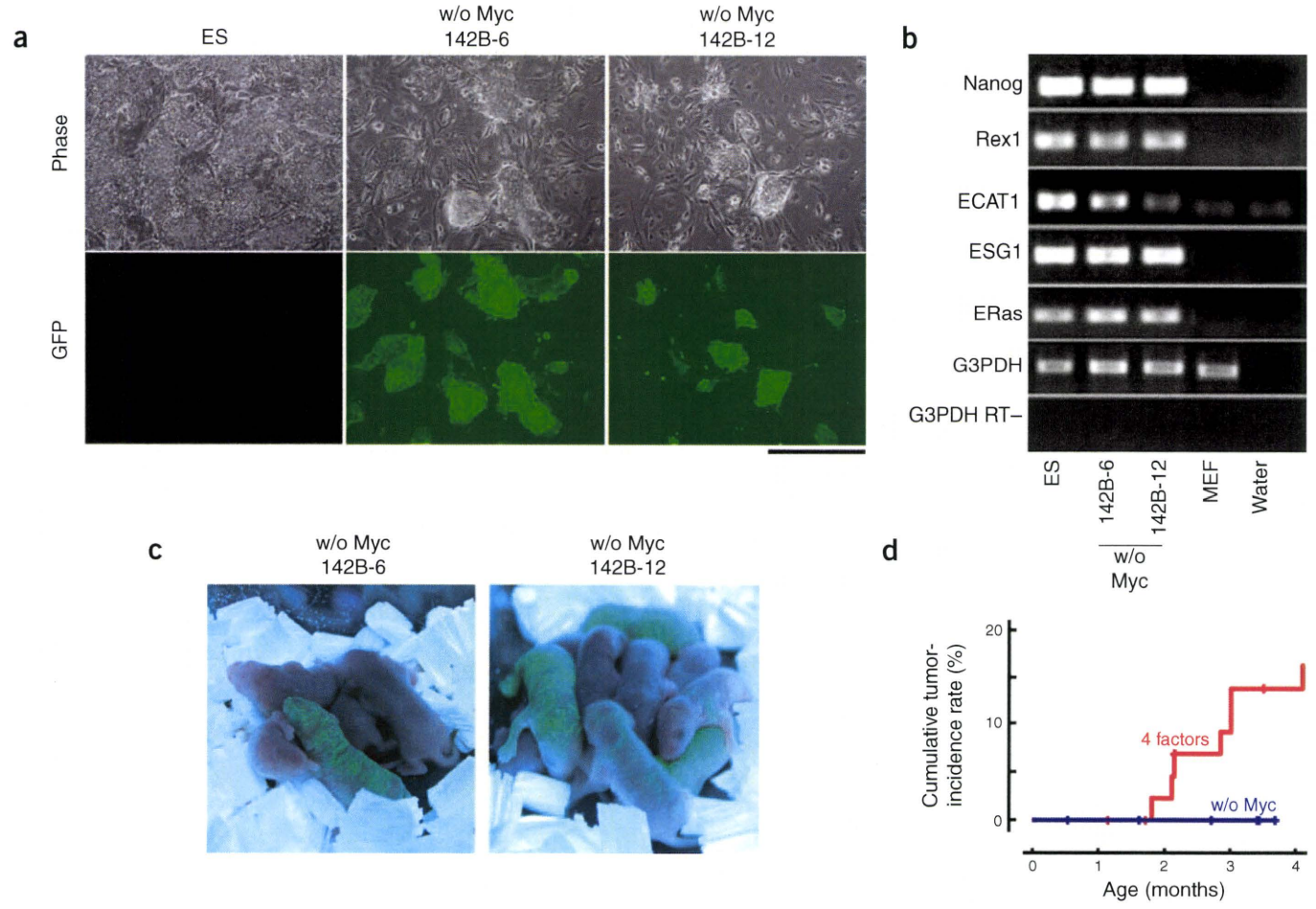

Figure 2 Generation of iPS cells without the Myc retrovirus from MEFs containing the Fbxo15 reporter and the constitutively active GFP transgene. (**a**) Morphology of iPS cells generated without the Myc retrovirus, using phase contrast microscopy. The bar indicates 500 μm. (**b**) RT-PCR analyses of ES-cell marker genes in ES, MEF and iPS cells generated without Myc. (**c**) Chimeras derived from iPS cells induced without Myc (clones 142B-6 and 142B-12). (**d**) The incidence of tumor-associated death in chimeras derived from iPS cells, which were generated with or without Myc.

in a patchy manner. DsRed was detected in only a small portion of some colonies, indicating that it was largely silenced. No overlap was observed between GFP and DsRed expression. Most of these colonies were expandable and produced iPS cells, which became positive for GFP and negative for DsRed at passage 2. Therefore, the omission of Myc resulted in a more specific generation of iPS cells, in which Nanog-GFP is activated and the retroviruses are silenced.

We next attempted to generate iPS cells from adult TTFs that did not have selection markers but had the DsRed transgene driven by a constitutively active promoter[13]. The four factors or the three factors devoid of Myc were introduced. In addition, a GFP retrovirus was introduced to monitor silencing. After 30 d without drug selection, ~1,000 colonies emerged from 0.5×10^5 cells transduced with the four factors. Most of them were positive for GFP, indicating that retroviral silencing did not take place in these cells. In contrast, only 16 colonies (**Fig. 3b**) emerged from 3.5×10^5 cells transduced with the three factors devoid of Myc. Most of these colonies expressed no GFP, and the remaining colonies expressed GFP in small areas. All of these colonies were expandable and showed ES cell–like morphology at the second passage. They were all negative for GFP, thus indicating retroviral silencing. RT-PCR showed that these cells expressed ES-cell marker genes at comparable levels to those in ES cells (**Fig. 3c**). In addition, RT-PCR confirmed the retroviral silencing of Klf4 and the absence of the Myc transgene in iPS cells generated with the three factors. Furthermore, when transplanted into blastocysts, these cells gave rise to chimeras (**Fig. 3d** and **Supplementary Table 1**). Therefore, by omitting MYC, high-quality iPS cells can be efficiently generated from adult TTFs without drug selection.

We have recently reported the generation of iPS cells from adult human dermal fibroblasts (hDFs) by the same four factors[14]. We therefore examined whether human iPS cells can be generated without the MYC retrovirus. As we described, from 5×10^4 hDFs transduced with the four factors, we obtained ~10 human (h)ES cell–like colonies and ~100 non-hES cell–like colonies (**Fig. 4a**). Without MYC, we obtained no colonies at all. From 5×10^5 hDFs transduced with the four factors, we obtained >500 non-hES cell–like colonies. We occasionally observed a few hES cell–like colonies, but it was difficult to isolate these cells because of the high number of background cells. Without MYC, we obtained 0–5 hES cell–like colonies with a few background cells. The hES cell–like colonies without MYC were expandable and were positive for hES-cell markers, including SSEA-3, SSEA-4, TRA-1-60, TRA-1-81, TRA-2-49/6E and NANOG (**Fig. 4b**). RT-PCR showed that the cells expressed hES-cell marker genes such as the endogenous OCT3/4, the endogenous SOX2, NANOG

and REX1 at similar levels to those in hES cell line H9 and human embryonic carcinoma cell line NTERA-2 (**Fig. 4c**). Furthermore, these cells differentiated into various cells that were positive for α-smooth muscle actin (SMA), βIII-tubulin and α-fetoprotein (AFP) (**Fig. 4d**). Thus, as is the case with mouse iPS cells, the omission of MYC resulted in a more specific induction of adult human fibroblasts to iPS cells, but with lower efficiency.

Our study does not argue that Myc is dispensable for iPS cell generation. We found that MEFs expressed c-Myc from the endogenous gene at ~20% of the levels observed in mouse ES cells (**Supplementary Fig. 3** online). This expression continues in iPS cells. Thus, Oct3/4, Sox2 and Klf4 may recruit endogenous Myc proteins to induce reprogramming. The endogenous expression levels may increase during the course of reprogramming. Recently, another group reported the generation of human iPS cells from neonate fibroblasts by a different combination of OCT3/4, SOX2, NANOG and LIN28 (ref. 15). Whether the same four factors work with adult human fibroblasts remains to be determined. In addition, LIN28 may activate endogenous Myc proteins by enhancing translation of insulin-like growth factor-2 (ref. 16). Further studies are required to determine the roles of Myc and the other factors in the reprogramming process.

In summary, we have demonstrated that iPS cells can be generated from mouse and human fibroblasts without the Myc retrovirus. Mice derived from iPS cells that had not been transduced with the Myc retrovirus showed a significantly reduced incidence of tumorigenicity compared with those derived from cells transduced with the four factors. Without the Myc retrovirus, however, the efficiency of iPS cell generation decreased substantially. In approximately half

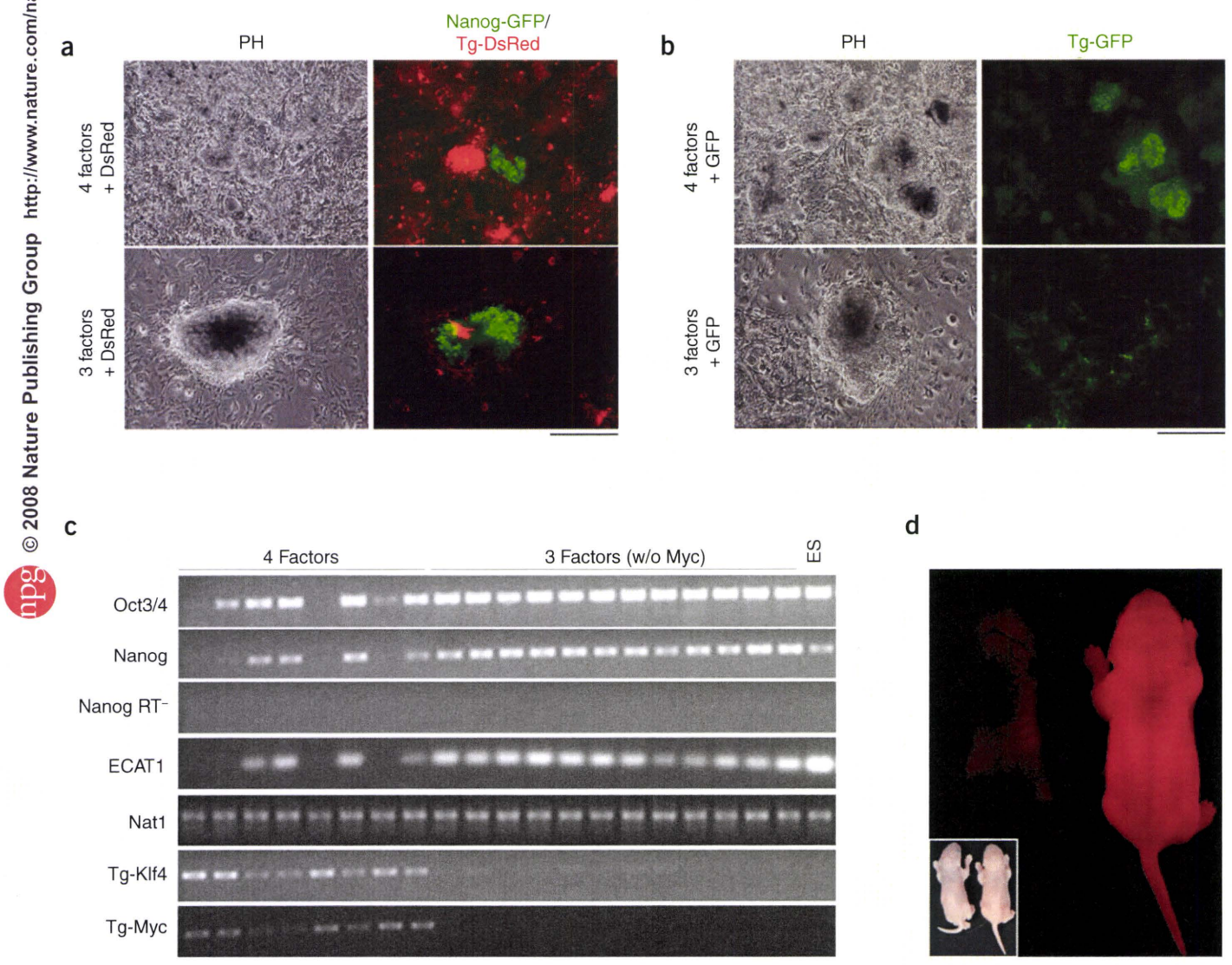

Figure 3 The efficient isolation of iPS cells without drug selection. (**a**) Morphology of iPS cells induced from adult TTFs containing the Nanog-GFP-IRES-Puro^r reporter. Cells were transduced with either the four factors or the three factors devoid of Myc, together with DsRed, and then were cultured for 30 d without drug selection. Expression of the Nanog reporter (Nanog-GFP) and the DsRed retrovirus (Tg-DsRed) was examined by fluorescence microscopy. The bar indicates 500 μm. (**b**) Morphology of iPS cells induced from adult TTFs, which contained a DsRed transgene driven by a constitutively active promoter (ACTB, β-actin gene) but lacked the Nanog- or Fbxo15- selection cassettes. The cells were transduced with either the four factors or the three factors devoid of Myc, together with GFP, and then cultured for 30 d without drug selection. The expression of the GFP retrovirus (Tg-GFP) was examined by fluorescence microscopy. The bar indicates 500 μm. (**c**) RT-PCR analyses of ES-cell marker genes in ES cells and in iPS cells generated from TTFs without drug selection (8 clones with four factors and 12 clones with three factors). (**d**) Chimeras derived from iPS cells, which were generated from adult TTFs without drug selection or the Myc retrovirus.

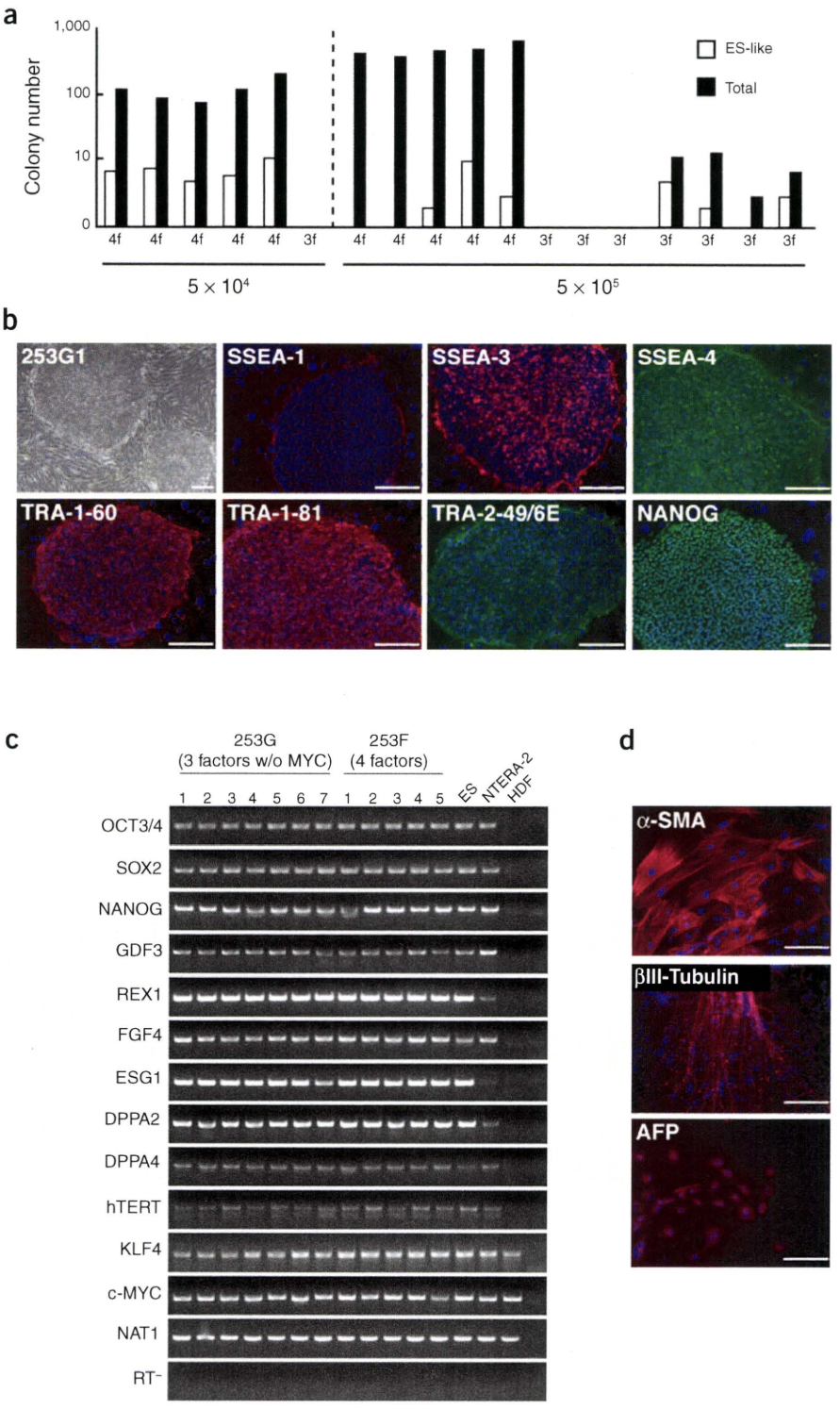

Figure 4 Generation of human iPS cells without the MYC retrovirus. (**a**) The number of hES cell–like colonies and total colonies from either 5×10^4 or 5×10^5 hDFs, which had been transduced either with the four factors or with the three factors without MYC. (**b**) The morphology and immunostaining of hES-cell markers in human iPS cells generated without MYC (clone 253G1). Bars, 100 μm. (**c**) The expression of ES-cell marker genes in human iPS cells derived from hDFs without the MYC retrovirus (253G) or with c-MYC (253F). (**d**) Embryoid body–mediated differentiation of human iPS cells generated without the MYC retrovirus (clone 253G1). Bars, 100 μm.

the experiments, we were not able to obtain human iPS cells when transduction with the Myc retrovirus was omitted. It will be important to find factors or small molecules that can enhance the efficiency of iPS cell generation without Myc for the generation of disease- and patient-specific iPS cells.

METHODS

Plasmid constructions. The coding regions of family genes were amplified by RT-PCR with the primers listed in **Supplementary Table 3** online, subcloned into pDONR201 or pENTR-D-TOPO (Invitrogen), and recombined with pMXs-gw by the LR reaction (Invitrogen).

Retroviral transduction. pMXs-based retroviral vectors were transfected into Plat-E cells[12] using Fugene 6 reagents (Roche) according to manufacturer's directions. Twenty-four hours after transfection, the medium was replaced. After 24 h, virus-containing supernatant was used for retroviral infection. In a 'mixed' protocol, the mixture of plasmids for the four factors was transfected into a single dish of Plat-E cells. In a 'separate' method, each plasmid was transfected into separate dishes of Plat-E cells. Virus-containing supernatant was mixed before transduction. Significantly higher transduction efficiency was observed with the separate method.

Induction of iPS cells with drug selection. The induction of iPS cells was performed as previously described[1,3] with some modifications. Briefly, MEFs, which contained either the Nanog-GFP-IRES-Puro^r reporter or the Fbxo15-βgeo reporter, or both, were seeded at 1.3 and 8.0×10^5 cells/well in 6-well plates and 100-mm dish, respectively, with SNL leukemia inhibitory factor feeder cells[17]. The transduced cells were cultivated with ES medium containing leukemia inhibitory factor[18]. Selection with G418 (300 μg/ml) or puromycin (1.5 μg/ml) was started as indicated. Twenty-five to 30 d after transduction, the number of colonies was recorded. Some colonies were then selected for expansion.

iPS cell generation without drug selection. TTFs were isolated from adult Nanog-reporter mice or adult DsRed-transgenic mice[13]. Retrovirus-containing supernatant was prepared in the separated method. For the four-factor transduction, retrovirus-containing supernatants for Klf4, c-Myc, Oct3/4, Sox2 and DsRed, were mixed with the ratio of 1:1:1:1:4. When the fibroblasts were transduced with the three factors, retrovirus-containing supernatants for Klf4, Oct3/4, Sox2, Mock and DsRed were mixed with the ratio of 1:1:1:1:4. With DsRed transgenic mice, the GFP retrovirus was used instead of DsRed. For transfection, TTFs were seeded at 8.0×10^5 cells per 100-mm dish, which did not have feeder cells. TTFs were incubated in the virus/polybrene -containing supernatants for 24 h. Four days after transduction, TTFs transduced with the three factors were reseeded at 3.5×10^5 cells per 100-mm dish with SNL feeder cells and cultured with ES medium. TTFs transduced with the four factors were reseeded at 0.5×10^5 cells per 100-mm dish with feeder cells. Thirty to 40 d after transduction, the colonies were selected for expansion.

Characterization of iPS cells. RT-PCR and teratoma formation were performed as previously described[1,3]. For the chimera experiments, 15–20 iPS cells were injected into BDF1-derived blastocysts, which were then transplanted into the uteri of pseudo-pregnant mice.

Generation of human iPS cells. DFs from the facial dermis of a 36-year-old Caucasian female were purchased from Cell Applications, Inc. Induction of iPS cells was performed as described[14].

Note: Supplementary information is available on the Nature Biotechnology website.

ACKNOWLEDGMENTS

We thank K. Yae and M. Maekawa for their valuable scientific discussions; M. Narita for technical assistance; and R. Kato and R. Iyama for administrative assistance. We also thank K. Tomoda for the RNA of hES cells, T. Kitamura for the Plat-E cells and pMXs retroviral vectors, and R. Farese for the RF8 ES cells. This study was supported in part by a grant from the Program for Promotion of Fundamental Studies in Health Sciences of NIBIO, a grant from the Leading Project of MEXT, a grant from Uehara Memorial Foundation and Grants-in-Aid for Scientific Research of JSPS and MEXT (to S.Y.). T. A. and K.O. are JSPS research fellows.

AUTHOR CONTRIBUTIONS

M.N., M.K., K.Tanabe, K.Takahashi, T.A. and K.O. generated and characterized iPS cells. T.I. performed the chimera experiments. Y.M. prepared plasmids. N.T. characterized iPS cells. S.Y. supervised the study and wrote the manuscript.

Published online at http://www.nature.com/naturebiotechnology/
Reprints and permissions information is available online at http://npg.nature.com/reprintsandpermissions/

1. Takahashi, K. & Yamanaka, S. Induction of pluripotent stem cells from mouse embryonic and adult fibroblast cultures by defined factors. *Cell* **126**, 663–676 (2006).
2. Wernig, M. *et al.* In vitro reprogramming of fibroblasts into a pluripotent ES cell-like state. *Nature* **448**, 318–324 (2007).
3. Okita, K., Ichisaka, T. & Yamanaka, S. Generation of germ-line competent induced pluripotent stem cells. *Nature* **448**, 313–317 (2007).
4. Maherali, N. *et al.* Directly reprogrammed fibroblasts show global epigenetic remodelling and widespread tissue contribution. *Cell Stem Cell* **1**, 55–70 (2007).
5. Chambers, I. *et al.* Functional expression cloning of nanog, a pluripotency sustaining factor in embryonic stem cells. *Cell* **113**, 643–655 (2003).
6. Mitsui, K. *et al.* The homeoprotein Nanog is required for maintenance of pluripotency in mouse epiblast and ES cells. *Cell* **113**, 631–642 (2003).
7. Ryan, A.K. & Rosenfeld, M.G. POU domain family values: flexibility, partnerships, and developmental codes. *Genes Dev.* **11**, 1207–1225 (1997).
8. Schepers, G.E., Teasdale, R.D. & Koopman, P. Twenty pairs of sox: extent, homology, and nomenclature of the mouse and human sox transcription factor gene families. *Dev. Cell* **3**, 167–170 (2002).
9. Dang, D.T., Pevsner, J. & Yang, V.W. The biology of the mammalian Kruppel-like family of transcription factors. *Int. J. Biochem. Cell Biol.* **32**, 1103–1121 (2000).
10. Adhikary, S. & Eilers, M. Transcriptional regulation and transformation by Myc proteins. *Nat. Rev. Mol. Cell Biol.* **6**, 635–645 (2005).
11. Tokuzawa, Y. *et al.* Fbx15 is a novel target of Oct3/4 but is dispensable for embryonic stem cell self-renewal and mouse development. *Mol. Cell. Biol.* **23**, 2699–2708 (2003).
12. Morita, S., Kojima, T. & Kitamura, T. Plat-E: an efficient and stable system for transient packaging of retroviruses. *Gene Ther.* **7**, 1063–1066 (2000).
13. Vintersten, K. *et al.* Mouse in red: red fluorescent protein expression in mouse ES cells, embryos, and adult animals. *Genesis* **40**, 241–246 (2004).
14. Takahashi, K. *et al.* Induction of pluripotent stem cells from adult human fibroblasts by defined factors. *Cell*, published online, doi:10.1016/j.cell.2007.11.019 (20 November 2007).
15. Yu, J. *et al.* Induced pluripotent stem cell lines derived from human somatic cells. *Science*, published online, doi:10.1126/science.1151526 (20 November 2007).
16. Polesskaya, A. *et al.* Lin-28 binds IGF-2 mRNA and participates in skeletal myogenesis by increasing translation efficiency. *Genes Dev.* **21**, 1125–1138 (2007).
17. McMahon, A.P. & Bradley, A. The Wnt-1 (int-1) proto-oncogene is required for development of a large region of the mouse brain. *Cell* **62**, 1073–1085 (1990).
18. Meiner, V.L. *et al.* Disruption of the acyl-CoA:cholesterol acyltransferase gene in mice: evidence suggesting multiple cholesterol esterification enzymes in mammals. *Proc. Natl. Acad. Sci. USA* **93**, 14041–14046 (1996).

nature biotechnology

BRIEF COMMUNICATIONS

Variation in the safety of induced pluripotent stem cell lines

Kyoko Miura[1–4], Yohei Okada[4,5], Takashi Aoi[1,3], Aki Okada[1], Kazutoshi Takahashi[1,3], Keisuke Okita[1,3], Masato Nakagawa[1–3], Michiyo Koyanagi[1,3], Koji Tanabe[1–3], Mari Ohnuki[1–3], Daisuke Ogawa[4], Eiji Ikeda[6], Hideyuki Okano[4] & Shinya Yamanaka[1–3,7]

We evaluated the teratoma-forming propensity of secondary neurospheres (SNS) generated from 36 mouse induced pluripotent stem (iPS) cell lines derived in 11 different ways. Teratoma-formation of SNS from embryonic fibroblast–derived iPS cells was similar to that of SNS from embryonic stem (ES) cells. In contrast, SNS from iPS cells derived from different adult tissues varied substantially in their teratoma-forming propensity, which correlated with the persistence of undifferentiated cells.

Many iPS cell clones have been generated using different transcription-factor combinations, tissues and selection methods, and some of these variables appear to influence teratoma formation after differentiation. Although mouse iPS cells produced with the transcription factors Oct3/4, Sox2, Klf4 and c-Myc[1] can contribute to germline-competent adult chimeras[2,3], these chimeras and their progeny often develop tumors owing to reactivation of the *c-Myc* transgene[2]. More recently, iPS cells were generated without *c-Myc* retroviruses, albeit with lower efficiency[4,5]. Chimeric mice derived from *c-Myc*$^-$ iPS cells showed substantially less tumor formation[4]. Chimera-competent iPS cells have been isolated by drug selection for the expression of pluripotency-associated genes such as *Nanog* and *Oct3/4* (also known as *Pouf51*; refs. 2,3) or without drug selection[6]. Moreover, iPS cells have also been derived from various tissues, including embryonic fibroblasts[2] and adult tail-tip fibroblasts (TTFs)[4], hepatocytes[7], gastric epithelial cells[7], pancreatic cells[8], neural stem cells[9–11] and B lymphocytes[12] in the mouse, and skin fibroblasts[13–15], keratinocytes[16] and peripheral blood cells[17] in the human. Considering all of the differences in reprogramming methods reported to date, the safety and therapeutic implications of these differences should be thoroughly evaluated before iPS cells are used in cell therapies[18].

In this study, we examined the effects of the *c-Myc* (also known as *Myc*) transgene, the tissue of origin and drug selection. We generated SNS from various mouse iPS cell clones and examined their neural differentiation capacity and teratoma-forming propensity after transplantation into the brains of nonobese/severe combined immunodeficient (NOD/SCID) mice. We used 36 iPS cell clones, characterized by (i) origin, that is, mouse embryonic fibroblast (MEF), TTF, hepatocyte or gastric epithelial cell; (ii) presence or absence of *c-Myc* retroviral transduction; and (iii) presence or absence of drug selection for *Nanog* or *Fbxo15* expression. The profiles and results of all the clones analyzed in this study are summarized in **Supplementary Tables 1** and **2**. PCR primers and antibodies used are summarized in **Supplementary Tables 3** and **4**. As controls, we used three ES cell clones: RF8 (ref. 19); a subclone (1A2) of RF8 carrying the *Nanog*-EGFP reporter[2]; and EB3 carrying the *Oct3/4* blasticidin-resistance reporter gene[20,21].

We generated neurospheres containing neural stem and progenitor cells from these iPS cells and ES cells using a published method[21] (**Supplementary Methods**). After embryoid body formation, most of the iPS clones and ES cells formed primary neurospheres in the presence of fibroblast growth factor 2; the primary neurospheres were then dissociated to form SNS (**Fig. 1a**). Three hepatocyte (Hep)-iPS clones and one gastric epithelial cell (Stm)-iPS cell clone failed to form neurospheres (**Supplementary Table 2**). Both iPS cell– and ES cell–derived SNS effectively differentiated into tri-lineage neural cells, that is, neurons, astrocytes and oligodendrocytes, *in vitro* (**Fig. 1b**) or *in vivo* (**Supplementary Fig. 1**).

To further assess the differentiation potential, we next examined how many undifferentiated cells persisted in SNS. We used MEF-iPS, TTF-iPS, Hep-iPS and ES cells containing the *Nanog*-EGFP reporter to detect undifferentiated cells by flow cytometry. The iPS cells were generated with or without the *c-Myc* retrovirus, and with or without drug selection for *Nanog* expression[2,4]. We found that SNS derived from MEF-iPS cells contained few *Nanog*-EGFP$^+$ cells regardless of the presence of the *c-Myc* retrovirus or the drug selection (0–0.38%). This result is similar to that of SNS derived from ES cells. By contrast, SNS from TTF-iPS cells had significantly ($P < 0.057$) higher amounts (0.025–20.1%) of *Nanog*-EGFP$^+$ undifferentiated cells than did those from MEF-iPS cells. SNS from Hep-iPS cells also contained higher amounts (0.034–12.0%) of *Nanog*-EGFP$^+$ undifferentiated cells (**Fig. 1c** and **Supplementary Fig. 2**). We found no significant effects of either the presence of *c-Myc* retrovirus (**Supplementary Fig. 3a**) or the drug selection (**Supplementary Fig. 3b**) on the proportion of *Nanog*-EGFP$^+$ cells in SNS.

To characterize the SNS *in vivo*, we transplanted them into the striata of NOD/SCID mice and examined tumor formation for up to 45 weeks (**Fig. 2a**, **Supplementary Fig. 4** and **Supplementary Methods**). We dissected the brains of animals that died or that became weak and were euthanized after transplantation. The remaining healthy mice were euthanized and dissected periodically 4–45 weeks after transplantation. In 34 mice transplanted with SNS derived from the three ES cell clones, three mice died or became weak because of tumors. On dissection, 31 mice showed no tumors and one mouse had a small tumor. Similar results were obtained with MEF-iPS cells. In 100 mice implanted with SNS from the 12 MEF-iPS cell clones, 9 mice died or became weak within 19 weeks after transplantation. In eight of these mice, we observed tumors. On dissection of the remaining mice, we observed that 66 mice did not have tumors, whereas 25 mice had tumors of various sizes.

[1]Center for iPS Cell Research and Application (CiRA), Kyoto University, Kyoto, Japan. [2]Department of Stem Cell Biology, Institute for Frontier Medical Sciences, Kyoto University, Kyoto, Japan. [3]Yamanaka iPS Cell Special Project, Japan Science and Technology Agency, Kawaguchi, Japan. [4]Department of Physiology, [5]Kanrinmaru-Project, [6]Department of Pathology, School of Medicine, Keio University, Tokyo, Japan. [7]Gladstone Institute of Cardiovascular Disease, San Francisco, California, USA. Correspondence should be addressed to H.O. (hidokano@sc.itc.keio.ac.jp) or S.Y. (yamanaka@frontier.kyoto-u.ac.jp).

Received 24 February; accepted 24 June; published online 9 July 2009; doi:10.1038/nbt.1554

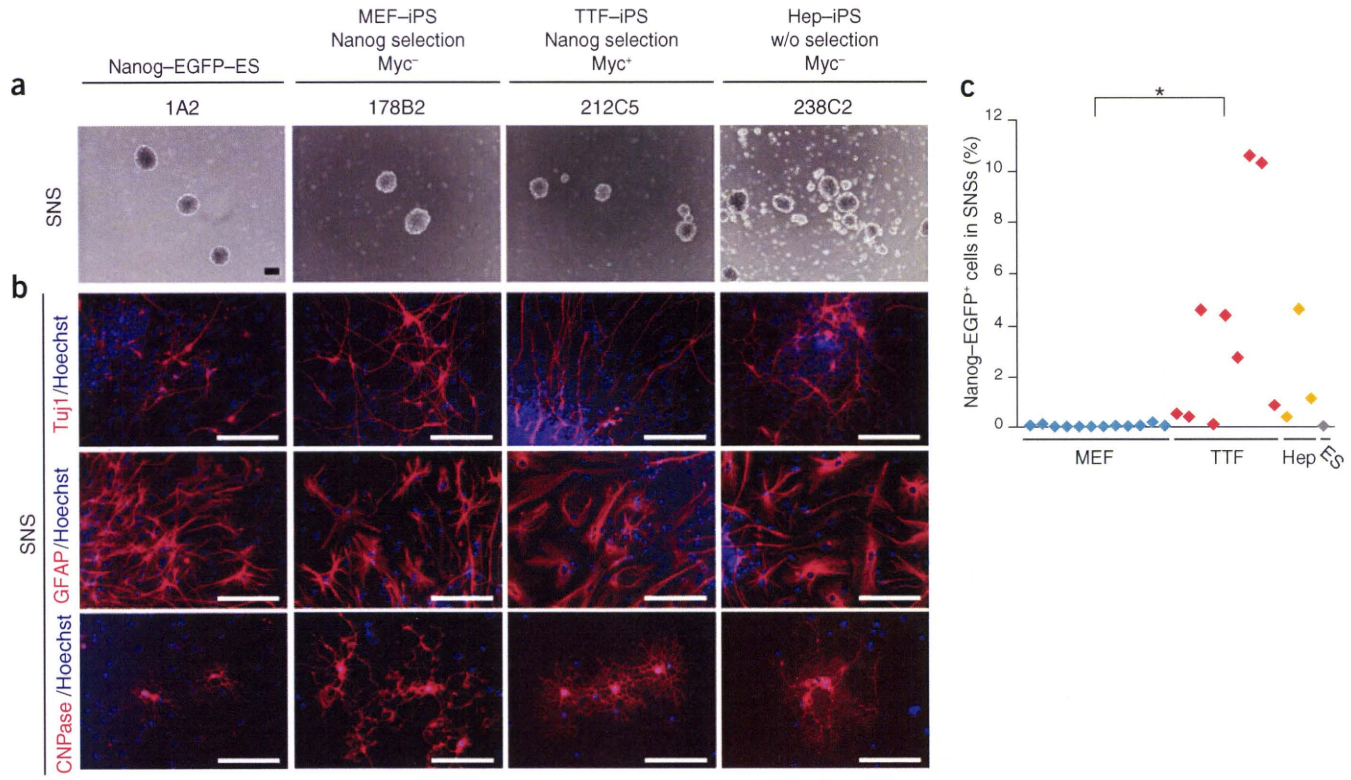

Figure 1 SNS formation from mouse iPS cells. (**a**) SNS derived from ES (1A2), MEF-iPS (178B2), TTF-iPS (212C5) and Hep-iPS cells (238C2). Scale bar, 200 μm. (**b**) Immunocytochemical analyses of cells differentiated from SNS for Tuj1 (neurons), GFAP (astrocytes) and CNPase (oligodendrocytes). Scale bars, 100 μm. (**c**) Comparison of the content of *Nanog*-EGFP$^+$ cells in SNS derived from ES cells, MEF-iPS cells, TTF-iPS cells and Hep-iPS cells.

By contrast, in 55 mice transplanted with SNS from 11 TTF-iPS cell clones, 46 mice died or became weak within 9 weeks after transplantation because of tumors. In the remaining nine healthy mice, no tumors were observed. Of 36 mice transplanted with seven Hep-iPS cell clones, 13 died or became weak within 17 weeks after transplantation. Ten of these mice developed tumors. In the remaining 23 healthy mice, no tumors were found on dissection. In addition, we transplanted two Stm-iPS cell clones into eight mice. No tumors were observed in these mice when they were dissected 16 weeks after transplantation.

We performed histological analyses of one tumor for each iPS cell clone whose SNS gave rise to tumors (**Supplementary Tables 1** and **2**). We found that all tumors examined contained large portions of undifferentiated cells, with small areas of differentiated cells such as striated muscle, duct-forming epithelial cells, keratinized epithelial cells, cartilage and neural cells (**Supplementary Fig. 5**). Thus, these tumors were considered to be teratomas or, if they contained large portions of undifferentiated cells, teratocarcinomas. In sectioned brains without tumors, we confirmed survival of grafted cells.

Statistical analyses showed that SNS from TTF-iPS cells produced significantly ($P < 0.01$) larger teratomas than did those from the other iPS cells or ES cells (**Fig. 2b**). In addition, SNS from TTF-iPS cells and Hep-iPS cells resulted in significantly ($P < 0.01$) higher incidence of weakness and death (**Fig. 2c**). We found no significant effects of either the presence of *c-Myc* retrovirus (**Supplementary Fig. 6a**) or the drug selection (**Supplementary Fig. 6b**) on the sizes of tumors or the incidence of weakness and death. By contrast, there was a significant ($P < 0.01$) correlation between teratoma diameter and the content of *Nanog*-EGFP$^+$ cells in SNS (**Fig. 2d**).

We have previously reported that tumors observed in iPS cell–derived chimeric mice were attributable to the reactivation of the *c-Myc* retrovirus[2]. In contrast, in the present study, use of the *c-Myc* retrovirus did not affect the teratoma-forming propensity of SNS (**Supplementary Fig. 6a**). Furthermore, we did not detect reactivation of *c-Myc* or other transgenes in SNS or teratomas (**Supplementary Fig. 7**). The mechanisms underlying the different teratoma-forming propensities of iPS cells remain to be determined.

The data presented here indicate that the teratoma-forming propensities of SNS vary significantly depending on the iPS cells' tissue of origin. SNS from TTF-iPS cells showed the highest propensity, whereas those from MEF-iPS cells and Stm-iPS cells showed the lowest, being comparable to those from ES cells. SNS from Hep-iPS cells showed an intermediate propensity. We note that teratoma formation by derivatives of iPS cells may be affected by the methods used for reprogramming and differentiation, the site of transplantation, the host background and other factors. For example, reprogramming methods that do not involve genomic integration have been reported to generate human iPS cells less susceptible to insertional mutagenesis[22,23]. All of the variables affecting safety must be rigorously evaluated before cell therapies based on iPS cells advance to the clinic.

Note: Supplementary information is available on the Nature Biotechnology website.

ACKNOWLEDGMENTS

We thank H. Abe, S. Yamaguchi, T. Tada, Y. Matsuzaki, T. Sunabori, H. Naka, M. Nishino, H. Higashi, T. Ichisaka and M. Imamura for technical assistance and scientific discussions. We also thank H. Niwa (CDB, RIKEN, JAPAN) for the EB3-ES cells, R. Farese (UCSF, USA) for the RF8 ES cells, A. Miyawaki (BSI, RIKEN, JAPAN) for the Venus gene and H. Miyoshi (BioResource Center, RIKEN, JAPAN) for the lentiviral vectors. This work was supported by grants from the Ministry of Education, Culture, Sports, Science and Technology of Japan; Japan Science and Technology Agency; National Institute of Biomedical Innovation; Japan Society for the Promotion of Science (JSPS), the Ministry of Health, Labor, and Welfare; the General Insurance Association of Japan and Keio Gijuku Academic Development Funds. K.M is supported by Research Fellowships for Young Scientists from JSPS.

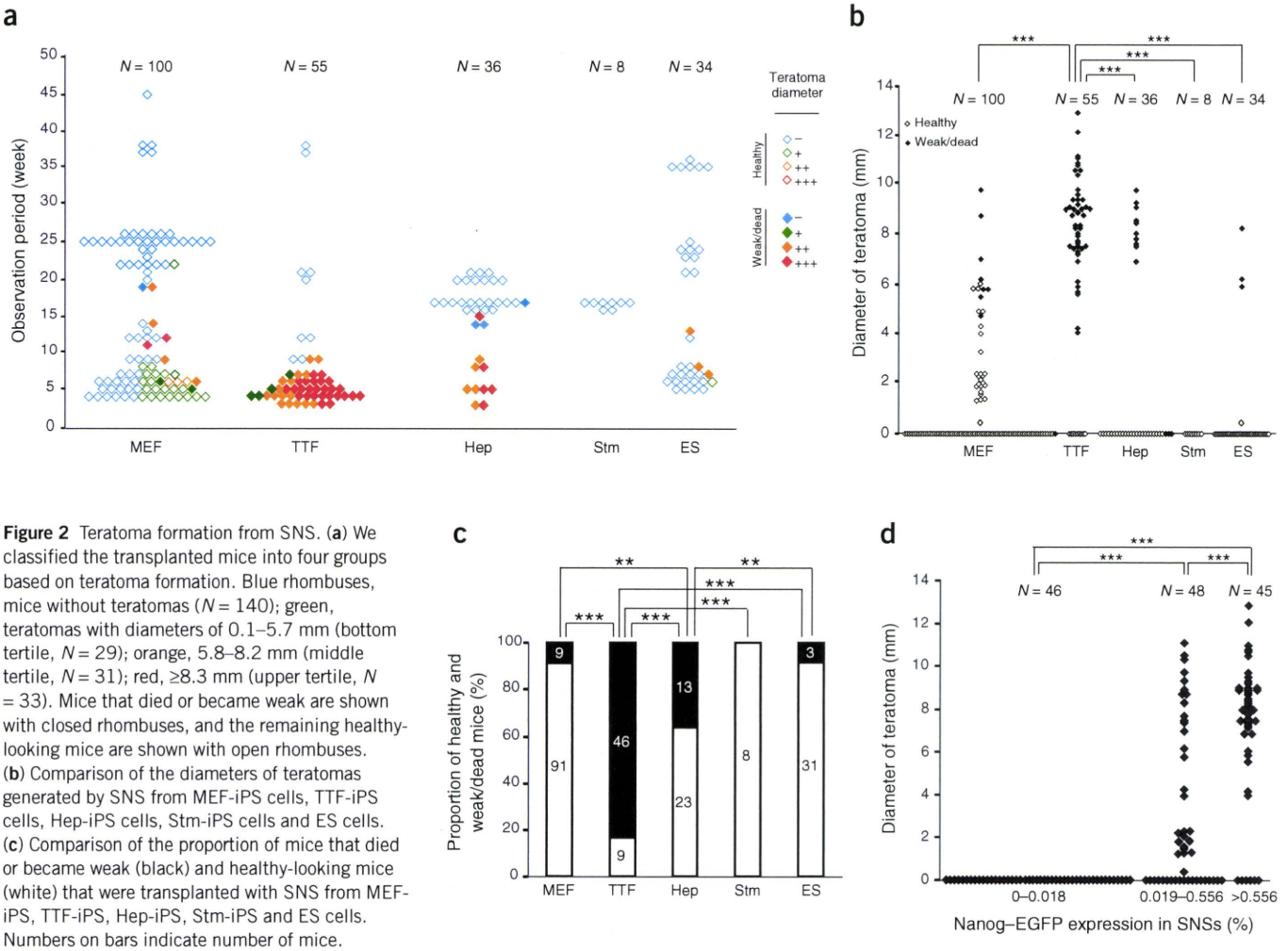

Figure 2 Teratoma formation from SNS. (**a**) We classified the transplanted mice into four groups based on teratoma formation. Blue rhombuses, mice without teratomas ($N = 140$); green, teratomas with diameters of 0.1–5.7 mm (bottom tertile, $N = 29$); orange, 5.8–8.2 mm (middle tertile, $N = 31$); red, ≥8.3 mm (upper tertile, $N = 33$). Mice that died or became weak are shown with closed rhombuses, and the remaining healthy-looking mice are shown with open rhombuses. (**b**) Comparison of the diameters of teratomas generated by SNS from MEF-iPS cells, TTF-iPS cells, Hep-iPS cells, Stm-iPS cells and ES cells. (**c**) Comparison of the proportion of mice that died or became weak (black) and healthy-looking mice (white) that were transplanted with SNS from MEF-iPS, TTF-iPS, Hep-iPS, Stm-iPS and ES cells. Numbers on bars indicate number of mice. (**d**) Correlation between the content of *Nanog*-EGFP$^+$ cells in iPS cell–derived SNS and the diameters of teratomas produced by the SNS. Mice transplanted with the SNS were grouped according to the percentage of *Nanog*-EGFP$^+$ cells (0–0.018%, bottom tertile (46 mice); 0.019–0.556%, middle tertile (48 mice); >0.556%, upper tertile (45 mice)). All procedures were approved by the ethics committee of Kyoto University and Keio University, which were in accordance with the Guide for the Care and Use of Laboratory Animals (US National Institutes of Health).

AUTHOR CONTRIBUTIONS

K.M. conducted most of the experiments. Y.O., T.A., A.O. and M.N. supported experiments and analyses. K. Takahashi, T.A., K.O., M.K., K. Tanabe and M.O. prepared undifferentiated iPS cells. E.I. and K. Takahashi assisted with the pathological analyses. D.O. assisted in some of the stereotactic transplantations. S.Y. and H.O. supervised the entire project. K.M. and S.Y. wrote the manuscript.

Published online at http://www.nature.com/naturebiotechnology/.
Reprints and permissions information is available online at http://npg.nature.com/reprintsandpermissions/.

1. Takahashi, K. & Yamanaka, S. *Cell* **126**, 663–676 (2006).
2. Okita, K., Ichisaka, T. & Yamanaka, S. *Nature* **448**, 313–317 (2007).
3. Wernig, M. *et al. Nature* **448**, 318–324 (2007).
4. Nakagawa, M. *et al. Nat. Biotechnol.* **26**, 101–106 (2008).
5. Wernig, M., Meissner, A., Cassady, J.P. & Jaenisch, R. *Cell Stem Cell* **2**, 10–12 (2008).
6. Meissner, A., Wernig, M. & Jaenisch, R. *Nat. Biotechnol.* **25**, 1177–1181 (2007).
7. Aoi, T. *et al. Science* **321**, 699–702 (2008).
8. Stadtfeld, M., Brennand, K. & Hochedlinger, K. *Curr. Biol.* **18**, 890–894 (2008).
9. Silva, J. *et al. PLoS Biol.* **6**, e253 (2008).
10. Kim, J.B. *et al. Nature* **454**, 646–650 (2008).
11. Eminli, S., Utikal, J.S., Arnold, K., Jaenisch, R. & Hochedlinger, K. *Stem Cells* **26**, 2467–2474 (2008).
12. Hanna, J. *et al. Cell* **133**, 250–264 (2008).
13. Park, I.H. *et al. Nature* **451**, 141–146 (2008).
14. Yu, J. *et al. Science* **318**, 1917–1920 (2007).
15. Takahashi, K. *et al. Cell* **131**, 861–872 (2007).
16. Aasen, T. *et al. Nat. Biotechnol.* **26**, 1276–1284 (2008).
17. Loh, Y.H. *et al. Blood* **113**, 5476–5479 (2009).
18. Yamanaka, S. *Cell* **137**, 13–17 (2009).
19. Meiner, V.L. *et al. Proc. Natl. Acad. Sci. USA* **93**, 14041–14046 (1996).
20. Niwa, H., Masui, S., Chambers, I., Smith, A.G. & Miyazaki, J. *Mol. Cell. Biol.* **22**, 1526–1536 (2002).
21. Okada, Y. *et al. Stem Cells* **26**, 3086–3098 (2008).
22. Yu, J. *et al. Science* **324**, 797–801 (2009).
23. Kim, D.H. *et al. Cell Stem Cell* **4**, 472–476 (2009).

LETTERS

IGFBP-4 is an inhibitor of canonical Wnt signalling required for cardiogenesis

Weidong Zhu[1]*, Ichiro Shiojima[1]*, Yuzuru Ito[2]*, Zhi Li[1], Hiroyuki Ikeda[1], Masashi Yoshida[1], Atsuhiko T. Naito[1], Jun-ichiro Nishi[1], Hiroo Ueno[3], Akihiro Umezawa[4], Tohru Minamino[1], Toshio Nagai[1], Akira Kikuchi[5], Makoto Asashima[2,6,7] & Issei Komuro[1]

Insulin-like growth-factor-binding proteins (IGFBPs) bind to and modulate the actions of insulin-like growth factors (IGFs)[1]. Although some of the actions of IGFBPs have been reported to be independent of IGFs, the precise mechanisms of IGF-independent actions of IGFBPs are largely unknown[1,2]. Here we report a previously unknown function for IGFBP-4 as a cardiogenic growth factor. IGFBP-4 enhanced cardiomyocyte differentiation *in vitro*, and knockdown of *Igfbp4* attenuated cardiomyogenesis both *in vitro* and *in vivo*. The cardiogenic effect of IGFBP-4 was independent of its IGF-binding activity but was mediated by the inhibitory effect on canonical Wnt signalling. IGFBP-4 physically interacted with a Wnt receptor, Frizzled 8 (Frz8), and a Wnt co-receptor, low-density lipoprotein receptor-related protein 6 (LRP6), and inhibited the binding of Wnt3A to Frz8 and LRP6. Although IGF-independent, the cardiogenic effect of IGFBP-4 was attenuated by IGFs through IGFBP-4 sequestration. IGFBP-4 is therefore an inhibitor of the canonical Wnt signalling required for cardiogenesis and provides a molecular link between IGF signalling and Wnt signalling.

The heart is the first organ to form during embryogenesis, and abnormalities in this process result in congenital heart diseases, the most common cause of birth defects in humans[3]. Molecules that mediate cardiogenesis are of particular interest because of their potential use for cardiac regeneration[4,5]. Previous studies have shown that soluble growth factors such as bone morphogenetic proteins (BMPs), fibroblast growth factors (FGFs), Wnts and Wnt inhibitors mediate the tissue interactions that are crucial for cardiomyocyte specification[3,4]. We proposed that there might be additional soluble factors that modulate cardiac development and/or cardiomyocyte differentiation.

P19CL6 cells differentiate into cardiomyocytes with high efficiency in the presence of 1% dimethylsulphoxide (DMSO)[6]. We cultured P19CL6 cells with culture media conditioned by various cell types in the absence of DMSO, and screened the cardiogenic activity of the conditioned media. The extent of cardiomyocyte differentiation was assessed by the immunostaining with MF20 monoclonal antibody that recognizes sarcomeric myosin heavy chain (MHC). Among the several cell types tested, culture media conditioned by a murine stromal cell line OP9 induced cardiomyocyte differentiation of P19CL6 cells without DMSO treatment (Fig. 1a, left and middle panels). Increased MF20-positive area was accompanied by the induction of cardiac marker genes such as *αMHC*, *Nkx2.5* and *GATA-4*, and by the increased protein levels of cardiac troponin T (cTnT) (Fig. 1a, right panel). In contrast, culture media conditioned by COS7 cells, mouse embryonic fibroblasts, NIH3T3 cells, HeLa cells, END2 cells (visceral endoderm-like cells), neonatal rat cardiomyocytes and neonatal rat cardiac fibroblasts did not induce cardiomyocyte differentiation of P19CL6 cells in the absence of DMSO (Fig. 1a and data not shown). From these observations, we postulated that OP9 cells secrete one or more cardiogenic growth factors.

To identify an OP9-derived cardiogenic factor, complementary DNA clones isolated by a signal sequence trap method from an OP9 cell cDNA library[7] were tested for their cardiogenic activities by transient transfection. When available, recombinant proteins were also used to confirm the results. Among candidate factors tested, IGFBP-4 induced cardiomyocyte differentiation of P19CL6 cells, as demonstrated by the increase in MF20-positive area and the induction of cardiac markers (Fig. 1b). We also cultured P19CL6 cells with OP9-conditioned media pretreated with an anti-IGFBP-4 neutralizing antibody. The application of an anti-IGFBP-4 neutralizing antibody attenuated the efficiency of cardiomyocyte differentiation induced by OP9-conditioned media (Fig. 1c). These findings strongly suggest that IGFBP-4 is a cardiogenic factor secreted from OP9 cells.

Because IGFBPs have been characterized as molecules that bind to and modulate the actions of IGFs, we tested whether IGFBP-4 promotes cardiogenesis by either enhancing or inhibiting the actions of IGFs. We first treated P19CL6 cells with a combination of anti-IGF-I and IGF-II-neutralizing antibodies or a neutralizing antibody against type-I IGF receptor. If IGFBP-4 induces cardiomyocyte differentiation by inhibiting IGF signalling, treatment with these antibodies should induce cardiomyocyte differentiation and/or enhance the cardiogenic effects of IGFBP-4. In contrast, if IGFBP-4 promotes cardiogenesis by enhancing IGF signalling, treatment with these antibodies should attenuate IGFBP-4-mediated cardiogenesis. However, treatment with these antibodies did not affect the efficiency of IGFBP-4-induced cardiomyocyte differentiation (Fig. 1d and data not shown). Treatment of P19CL6 cells with IGF-I and IGF-II also did not induce cardiomyocyte differentiation (data not shown). Furthermore, treatment with an IGFBP-4 mutant (IGFBP-4-H74P; His 74 replaced by Pro)[8] that is unable to bind IGFs induced cardiomyocyte differentiation of P19CL6 cells even more efficiently than wild-type IGFBP-4 (Fig. 1e). This is presumably due to the sequestration of wild-type IGFBP-4 but not mutant IGFBP-4-H74P by endogenous IGFs. In agreement with this idea, exogenous IGFs attenuated wild-type IGFBP-4-induced but not IGFBP-4-H74P-induced cardiogenesis (Fig. 1f). Taken together, these observations indicate

[1]Department of Cardiovascular Science and Medicine, Chiba University Graduate School of Medicine, Chiba 260-8670, Japan. [2]ICORP Organ Regeneration Project, Japan Science and Technology Agency (JST), Tokyo 153-8902, Japan. [3]Institute of Stem Cell Biology and Regenerative Medicine, Stanford University School of Medicine, Stanford, California 94305, USA. [4]Department of Reproductive Biology, National Institute for Child Health and Development, Tokyo 157-8535, Japan. [5]Department of Biochemistry, Graduate School of Biomedical Sciences, Hiroshima University, Hiroshima 734-8551, Japan. [6]Department of Life Sciences (Biology), Graduate School of Arts and Science, The University of Tokyo, Tokyo 153-8902, Japan. [7]National Institute of Advanced Industrial Sciences and Technology (AIST), Ibaraki 305-8562, Japan.
*These authors contributed equally to this work.

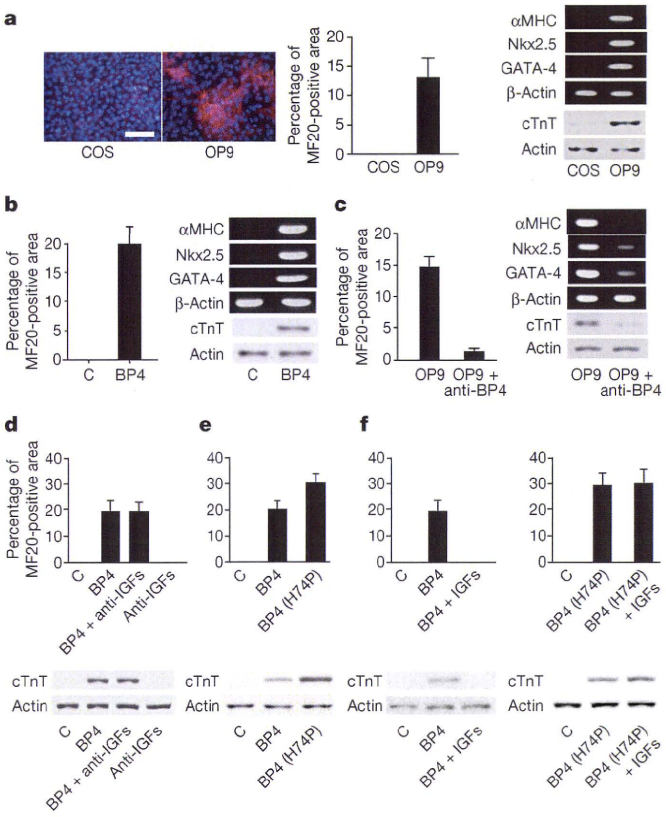

Figure 1 | IGFBP-4 promotes cardiomyocyte differentiation in an IGF-independent manner. **a**, Culture media conditioned by OP9 cells but not by COS7 cells induced cardiomyocyte differentiation of P19CL6 cells as assessed by MF20-positive area, cardiac marker-gene expression and cTnT protein expression. Scale bar, 100 μm. Error bars show s.d. **b**, Treatment with IGFBP-4 (1 μg ml^{-1}) induced cardiomyocyte differentiation of P19CL6 cells in the absence of DMSO. Error bars show s.d. **c**, Treatment with a neutralizing antibody against IGFBP-4 (anti-BP4; 40 μg ml^{-1}) attenuated cardiomyocyte differentiation of P19CL6 cells induced by OP9-conditioned media. Error bars show s.d. **d**, Treatment with neutralizing antibodies against IGF-I and IGF-II (anti-IGFs; 5 μg ml^{-1} each) had no effect on IGFBP-4-induced cardiomyocyte differentiation of P19CL6 cells. Error bars show s.d. **e**, Mutant IGFBP-4 (BP4(H74P)) that is incapable of binding to IGFs retained cardiomyogenic activity. Error bars show s.d. **f**, IGFs (100 ng ml^{-1} each) attenuated wild-type IGFBP-4-induced but not mutant IGFBP-4-H74P-induced cardiomyocyte differentiation of P19CL6 cells. Error bars show s.d.

that IGFBP-4 induces cardiomyocyte differentiation in an IGF-independent fashion.

To explore further the mechanisms by which IGFBP-4 induces cardiomyogenesis, we tested the hypothesis that IGFBP-4 might modulate the signals activated by other secreted factors implicated in cardiogenesis. It has been shown that canonical Wnt signalling is crucial in cardiomyocyte differentiation[3,4]. In P19CL6 cells, Wnt3A treatment activated β-catenin-dependent transcription of the TOPFLASH reporter gene, and this activation was attenuated by IGFBP-4 (Fig. 2a). Wnt/β-catenin signalling is transduced by the cell-surface receptor complex consisting of Frizzled and low-density-lipoprotein receptor (LDLR)-related protein 5/6 (LRP5/6)[9] and IGFBP-4 attenuated TOPFLASH activity enhanced by the expression of LRP6 or Frizzled 8 (Frz8) (Fig. 2a). As a control, IGFBP-4 did not alter BMP-mediated activation of a BMP-responsive reporter BRE–luc (Supplementary Fig. 1b). These findings suggest that IGFBP-4 is a specific inhibitor of the canonical Wnt pathway. To examine this possibility *in vivo*, we performed axis duplication assays in *Xenopus* embryos. Injection of *Xwnt8* or *Lrp6* mRNA caused secondary axis formation, and injection of *Xenopus IGFBP-4* (*XIGFBP-4*) mRNA alone had minimal effects on axis formation. However, Xwnt8-induced or LRP6-induced secondary axis formation was efficiently blocked by coexpression of XIGFBP-4 (Fig. 2b, c), indicating that IGFBP-4 inhibits canonical Wnt signalling *in vivo*. To explore the mechanisms of Wnt inhibition by IGFBP-4, *Xenopus* animal cap assays and TOPFLASH reporter gene assays were performed. In animal cap assays, IGFBP-4 inhibited LRP6-induced but not β-catenin-induced Wnt-target gene expression (Supplementary Fig. 1c). Similarly, IGFBP-4 attenuated Wnt3A-induced or LRP6-induced TOPFLASH activity but did not alter Dishevelled-1 (Dvl-1)-induced, LiCl-induced or β-catenin-induced TOPFLASH activity (Supplementary Fig. 1d, e). These findings suggest that IGFBP-4 inhibits canonical Wnt signalling at the level of cell-surface receptors. To examine whether IGFBP-4 antagonizes Wnt signalling via direct physical interaction with LRP5/6 or Frizzled, we produced conditioned media containing the Myc-tagged extracellular portion of LRP6 (LRP6N–Myc), the Myc-tagged cysteine-rich domain (CRD) of Frz8 (Frz8CRD–Myc), and V5-tagged IGFBP-4 (IGFBP-4–V5). Immunoprecipitation (IP)/western blot experiments revealed that IGFBP-4 interacted with LRP6N (Fig. 2d) and Frz8CRD (Fig. 2e). A liquid-phase binding assay with ^{125}I-labelled IGFBP-4 and conditioned media containing LRP6N–Myc or Frz8CRD–Myc demonstrated that the interaction between IGFBP-4 and LRP6N or Frz8CRD was specific and saturable (Fig. 2f, g). A Scatchard plot analysis revealed two binding sites with different binding affinities for LRP6N (Fig. 2f, inset) and a single binding site for Frz8CRD (Fig. 2g, inset). A similar binding assay with ^{125}I-labelled Wnt3A demonstrated that IGFBP-4 inhibited Wnt3A binding to LRP6N (Fig. 2h) and Frz8CRD (Fig. 2i), and a Lineweaver–Burk plot revealed that IGFBP-4 was a competitive inhibitor of the binding of Wnt3A to Frz8CDR (Supplementary Fig. 2a). IP/western blot analyses with various deletion mutants of LRP6 and IGFBP-4 revealed that IGFBP-4 interacted with multiple domains of LRP6 and that the carboxy-terminal thyroglobulin domain of IGFBP-4 was required for IGFBP-4 binding to LRP6 or Frz8CRD (Supplementary Fig. 2b–f). It has been shown that inhibition of canonical Wnt signalling promotes cardiomyocyte differentiation in embryonic stem (ES) cells and in chick, *Xenopus* and zebrafish embryos[4,10,11]. These results therefore collectively suggest that IGFBP-4 promotes cardiogenesis by antagonizing the Wnt/β-catenin pathway through direct interactions with Frizzled and LRP5/6.

Next we investigated the role of endogenous IGFBP-4 in P19CL6 cell differentiation into cardiomyocytes. Reverse transcriptase-mediated polymerase chain reaction (RT–PCR) analysis revealed that the expression of *Igfbp4* was upregulated during DMSO-induced P19CL6 cell differentiation (Fig. 3a). Expression of *Igfbp3* and *Igfbp5* was also upregulated in the early and the late phases of differentiation, respectively. Expression of *Igfbp2* was not altered, and that of *Igfbp1* or *Igfbp6* was not detected. When IGFBP-4 was knocked down by two different small interfering RNA (siRNA) constructs, DMSO-induced cardiomyocyte differentiation was inhibited in both cases (Fig. 3b). In contrast, knockdown of *Igfbp3* or *Igfbp5* did not inhibit DMSO-induced cardiomyocyte differentiation (Fig. 3b, right panel). Treatment with an anti-IGFBP-4 neutralizing antibody also blocked DMSO-induced cardiomyocyte differentiation (Fig. 3c). Secretion of endogenous IGFBP-4 is therefore required for the differentiation of P19CL6 cells into cardiomyocytes. Immunostaining for IGFBP-4 revealed that cardiac myocytes were surrounded by the IGFBP-4-positive cells, suggesting that a paracrine effect of IGFBP-4 on cardiomyocyte differentiation is predominant (Fig. 3d). Essentially the same results were obtained in ES cells (Supplementary Fig. 3d–g). To investigate whether IGFBP-4 promotes the differentiation of P19CL6 cells into cardiomyocytes by the inhibition of the canonical Wnt pathway, we expressed dominant-negative LRP6 (LRP6N) in P19CL6 cells. Expression of LRP6N enhanced cardiomyocyte differentiation of P19CL6 cells and reversed the inhibitory effect of *Igfbp4*

knockdown on cardiomyogenesis (Fig. 3e). These observations suggest that endogenous IGFBP-4 is required for cardiomyocyte differentiation of P19CL6 cells and ES cells, and that the cardiogenic effect of IGFBP-4 is mediated by its inhibitory effect on Wnt/β-catenin signalling.

The role of endogenous IGFBP-4 in cardiac development *in vivo* was also examined with *Xenopus* embryos. Whole-mount *in situ* hybridization analysis revealed that strong expression of *XIGFBP-4* was detected at stage 38 in the anterior part of the liver adjacent to the heart (Fig. 4a). Knockdown of *XIGFBP-4* by two different morpholino (MO) constructs resulted in cardiac defects, with more than 70% of the embryos having a small heart or no heart (Fig. 4b). The specificity of MO was confirmed by the observation that simultaneous injection of MO-resistant *XIGFBP-4* cDNA rescued the MO-induced cardiac defects (Fig. 4b, Supplementary Fig. 4c). Coexpression of IGF-binding-defective XIGFBP-4 mutant (XIGFBP-4-H74P) or dominant-negative LRP6 (LRP6N) also rescued the cardiac defects induced by *XIGFBP-4* knockdown (Fig. 4b), whereas overexpression of Xwnt8 in the heart-forming region resulted in cardiac defects similar to those induced by *XIGFBP-4* knockdown (Supplementary Fig. 4d–f), supporting the notion that the cardiogenic effect of IGFBP-4 is independent of IGFs but is mediated by inhibition of the Wnt/β-catenin pathway. The temporal profile of cardiac defects induced by *XIGFBP-4* knockdown was also examined by *in situ* hybridization with *cardiac troponin I* (*cTnI*) (Fig. 4c). At stage 34, morphology of the heart was comparable between control embryos and MO-injected embryos. However, at stage 38, when *XIGFBP-4* starts to be expressed in the anterior part of the liver, the expression of *cTnI* was markedly attenuated in MO-injected embryos; expression of *cTnI* was diminished and no heart-like structure was observed at stage 42. Thus, the heart is initially formed but its subsequent growth is perturbed in the absence of XIGFBP-4, suggesting that IGFBP-4

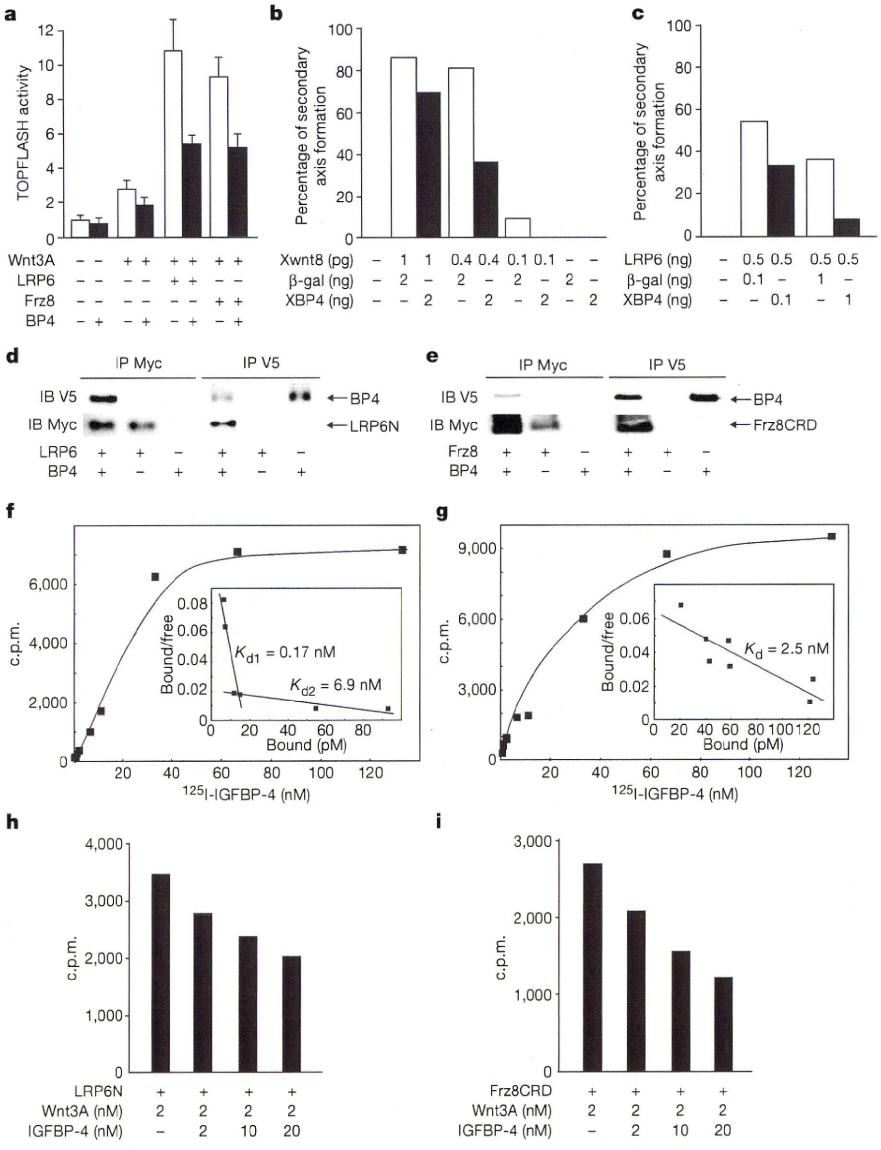

Figure 2 | IGFBP-4 inhibits Wnt/β-catenin signalling through direct interactions with Wnt receptors. **a**, IGFBP-4 attenuated β-catenin-dependent transcription in P19CL6 cells. P19CL6 cells were transfected with TOPFLASH reporter gene and expression vectors for LRP6 or Frz8, and then treated with Wnt3A or Wnt3A plus IGFBP-4; luciferase activities were then measured. Error bars show s.d. **b**, XIGFBP-4 (XBP4) inhibited Xwnt8-induced secondary-axis formation in *Xenopus* embryos ($n = 20$ for each group). **c**, IGFBP-4 inhibited LRP6-induced secondary-axis formation in *Xenopus* embryos ($n = 30$ for each group). **d**, **e**, IGFBP-4 interacted directly with LRP6N (**d**) and Frz8CRD (**e**). IB, immunoblotting; IP, immunoprecipitation. **f**, A binding assay between ^{125}I-labelled IGFBP-4 and LRP6N. The inset is a Scatchard plot showing two binding sites with different binding affinities. **g**, A binding assay between ^{125}I-labelled IGFBP-4 and Frz8CRD. The inset is a Scatchard plot showing a single binding site. **h**, **i**, IGFBP-4 inhibited Wnt3A binding to LRP6N (**h**) or Frz8CRD (**i**). ^{125}I-labelled Wnt3A binding to LRP6N or Frz8CRD was assessed in the presence of increasing amounts of IGFBP-4.